straightjacket is required for the synaptic stabilization of *cacophony*, a voltage-gated calcium channel α_1 subunit

Cindy V. Ly,[1] Chi-Kuang Yao,[2,3] Patrik Verstreken,[2,3] Tomoko Ohyama,[2] and Hugo J. Bellen[1,2,3,4]

[1]Department of Neuroscience, [2]Department of Molecular and Human Genetics, [3]Howard Hughes Medical Institute, and [4]Program in Developmental Biology, Baylor College of Medicine, Houston, TX 77030

In a screen to identify genes involved in synaptic function, we isolated mutations in *Drosophila melanogaster straightjacket* (*stj*), an $\alpha_2\delta$ subunit of the voltage-gated calcium channel. *stj* mutant photoreceptors develop normal synaptic connections but display reduced "on–off" transients in electroretinogram recordings, indicating a failure to evoke postsynaptic responses and, thus, a defect in neurotransmission. *stj* is expressed in neurons but excluded from glia. Mutants exhibit endogenous seizure-like activity, indicating altered neuronal excitability. However, at the synaptic level, *stj* larval neuromuscular junctions exhibit approximately fourfold reduction in synaptic release compared with controls stemming from a reduced release probability at these synapses. These defects likely stem from destabilization of Cacophony (Cac), the primary presynaptic α_1 subunit in *D. melanogaster*. Interestingly, neuronal overexpression of *cac* partially rescues the viability and physiological defects in *stj* mutants, indicating a role for the $\alpha_2\delta$ Ca^{2+} channel subunit in mediating the proper localization of an α_1 subunit at synapses.

Introduction

Neuronal voltage-gated calcium channels (VGCCs) mediate neuronal migration (Komuro and Rakic, 1998), neurite outgrowth (Rieckhof et al., 2003), synaptogenesis (Bahls et al., 1998), neuronal excitability (Pietrobon, 2005), and neurotransmission (Smith and Augustine, 1988; Robitaille et al., 1990). VGCCs are comprised of a pore-forming α_1 subunit associated with accessory subunits $\alpha_2\delta$, β, and γ (Takahashi et al., 1987; Tanabe et al., 1987). $\alpha_2\delta$ consists of two disulfide-linked subunits, α_2 and δ, derived from posttranslational cleavage of a single gene product (Ellis et al., 1988; De Jongh et al., 1990). Although δ is a minimal transmembrane domain that anchors the subunit to the plasma membrane, α_2 is extracellular and heavily glycosylated, a modification important for regulating α_1 activity (Jay et al., 1991; Gurnett et al., 1996; Sandoval et al., 2004).

Correspondence to H. Bellen: hbellen@bcm.tmc.edu

P. Verstreken's present address is VIB Department of Developmental Genetics, K.U. Leuven Center for Human Genetics, 3000 Leuven, Belgium.

Abbreviations used in this paper: Brp, Bruchpilot; Cac, Cacophony; CPG, central pattern generator; EJP, excitatory junctional potential; ERG, electroretinogram; mEJP, miniature EJP; NMJ, neuromuscular junction; PR, photoreceptor; SSR, subsynaptic reticulum; *stj*, *straightjacket*; TEM, transmission electron microscopy; TTX, tetrodotoxin; VGCC, voltage-gated calcium channel; VNC, ventral nerve cord; VWA, von Willebrand factor A.

The online version of this article contains supplemental material.

Our understanding of how $\alpha_2\delta$ affects α_1 pore subunits mostly derives from work in heterologous expression systems in which these subunits were coexpressed and biophysical parameters assessed by whole cell recording. Four $\alpha_2\delta$ homologues exist in vertebrates. Although several studies describe a role for $\alpha_2\delta_{1-3}$ in modulating the kinetics and voltage-dependence of channel gating (Singer et al., 1991; Felix et al., 1997; Klugbauer et al., 1999; Herlitze et al., 2003), others found no effect for $\alpha_2\delta$ in regulating these properties (Mikami et al., 1989; Gao et al., 2000). Research also suggests that $\alpha_2\delta_{1-2}$ increases Ca^{2+} currents (Singer et al., 1991; Felix et al., 1997; Klugbauer et al., 1999; Gao et al., 2000; Canti et al., 2005), and $\alpha_2\delta$ overexpression in nonneuronal cells enriches N-, P/Q-, and L-type channels at the plasma membrane (Felix et al., 1997; Canti et al., 2005). However, no current enhancement is observed when $\alpha_2\delta_1$ is coexpressed with R-type channels (Qin et al., 1998). Though these studies highlight the potential effects of $\alpha_2\delta$ on VGCCs, in vivo studies based on loss-of-function data should reveal the contribution of $\alpha_2\delta$ to regulation of native channels.

ducky mice that harbor mutations in $\alpha_2\delta_2$ have spike-wave seizures and are ataxic (Barclay et al., 2001; Brill et al., 2004; Donato et al., 2006). Also, dissociated *ducky* mutant Purkinje cells exhibit reduced Ca^{2+} currents (Barclay et al., 2001; Donato et al., 2006). Notably, gabapentin, an antiepileptic drug also used to

The Journal of Cell Biology, Vol. 181, No. 1, April 7, 2008 157–170
http://www.jcb.org/cgi/doi/10.1083/jcb.200712152

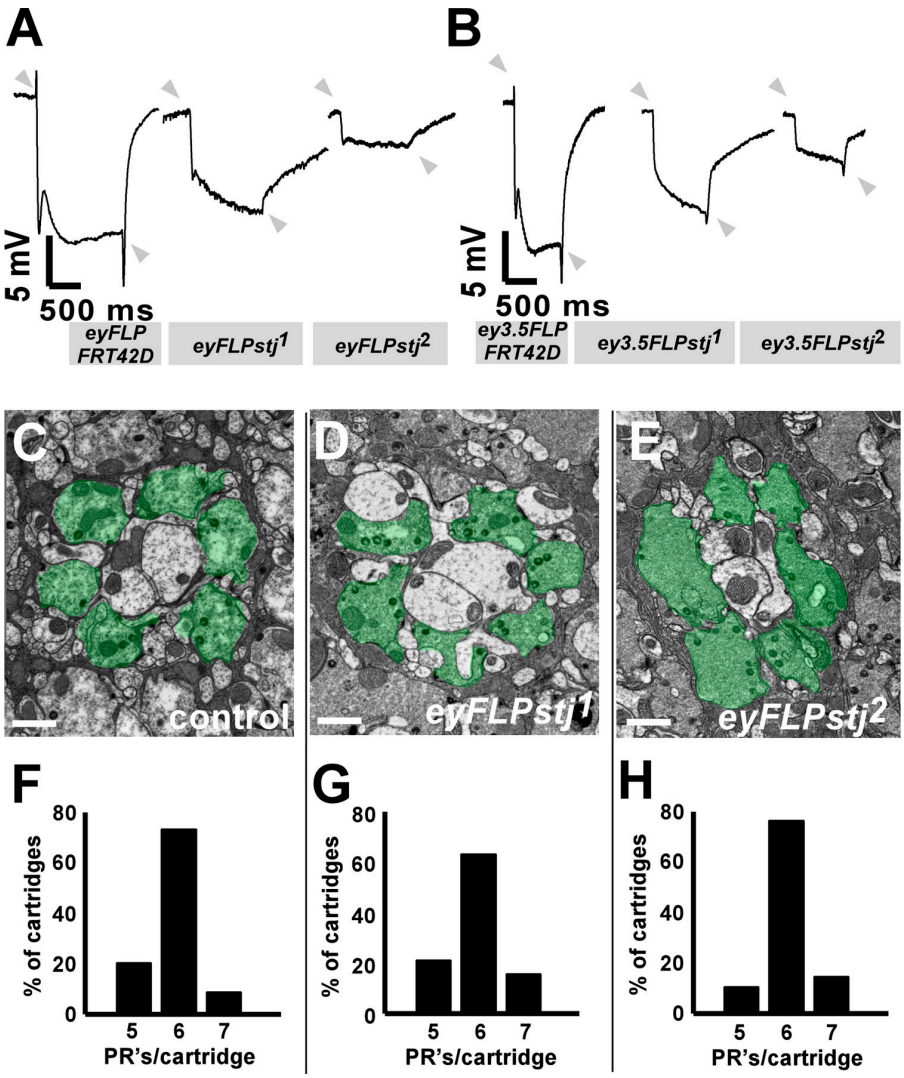

Figure 1. ***stj* mutant PRs have synaptic defects.** (A) ERGs from control (y w eyFLP GMR-lacZ; FRT42D/FRT42D cl2R w^+), eyFLPstj^1, and eyFLPstj^2 (y w eyFLP GMR-lacZ; FRT42D stj$^{1\text{ or }2}$/FRT42D cl2R w^+). On–off transients are indicated by arrowheads. (B) ERGs from control (y w ey3.5FLP; FRT42D/FRT42D cl2R w^+), ey3.5FLPstj^1, and ey3.5FLPstj^2 (y w ey3.5FLP; FRT42D stj$^{1\text{ or }2}$/FRT42D cl2R w^+), which render only PRs homozygous mutant. Arrowheads denote on–off transients. (C–E) TEM of laminar cartridges of control (C), eyFLPstj^1 (D), and eyFLPstj^2 (E). PR terminals are pseudo-colored green. Bars, 1 µm. (F–H) Histograms of PR sorting within cartridges for control (F), eyFLPstj^1 (G), and eyFLPstj^2 (H). 30 cartridges from three flies were quantified for each genotype.

treat neuropathic pain, binds specifically to $\alpha_2\delta$ (Gee et al., 1996), an interaction thought to reduce neurotransmission in these pathological conditions. Therefore, a better understanding of how $\alpha_2\delta$ subunits affect neurotransmission may shed insight into the mode of action of gabapentinoid drugs as well as VGCC function.

In a screen for genes affecting synaptic function, we identified *straightjacket* (*stj*), which encodes a *Drosophila melanogaster* $\alpha_2\delta$ similar to vertebrate $\alpha_2\delta_3$. *stj* mutants exhibit a severe reduction in Ca^{2+}-dependent evoked neurotransmitter release that stems from a presynaptic role for *stj* based on in situ hybridization studies, enhancer trap expression, and analysis of spontaneous release at mutant synapses. Furthermore, we observe a reduction of the primary presynaptic *D. melanogaster* α_1 subunit, Cacophony (Cac), at mutant synapses, indicating that the synaptic defects result from a failure to properly localize synaptic Ca^{2+} channels.

Results

stj mutants display electroretinogram (ERG) defects

In a forward genetic screen designed to isolate genes involved in synaptic function, we isolated three alleles in one complementation group. Using the *eyFLP* system (Stowers and Schwarz, 1999; Newsome et al., 2000), we made flies homozygous for randomly induced ethyl methanesulfonate mutations in the visual system that were otherwise heterozygous in the body, thus circumventing the lethality associated with many mutations affecting synaptic transmission. Mutant flies were behaviorally screened for a response to light in a phototaxis assay (Benzer, 1967). Flies with reduced phototaxis responses were crossed, and progeny with homozygous mutant eyes were subjected to ERG recordings (Pak et al., 1969), extracellular field recordings of the photoreceptor (PR) response to light. Although all mutants initially failed to phototax, this defect failed to persist in later generations (unpublished data), as observed for other mutants isolated in similar screens (Verstreken et al., 2003, 2005). However, in response to a light stimulus, *stj* mutants exhibit a reduced depolarization in the ERG, which suggests a defect in phototransduction, as well as a lack of "on–off" transients (Fig. 1 A, arrowheads), indicating a failure to induce a postsynaptic response (Pak et al., 1969). To determine whether the ERG defect stems from a pre- or postsynaptic requirement for the disrupted gene (the *eyFLP* system creates homozygous mutant PRs as well as mutant postsynaptic cells; Hiesinger et al., 2006),

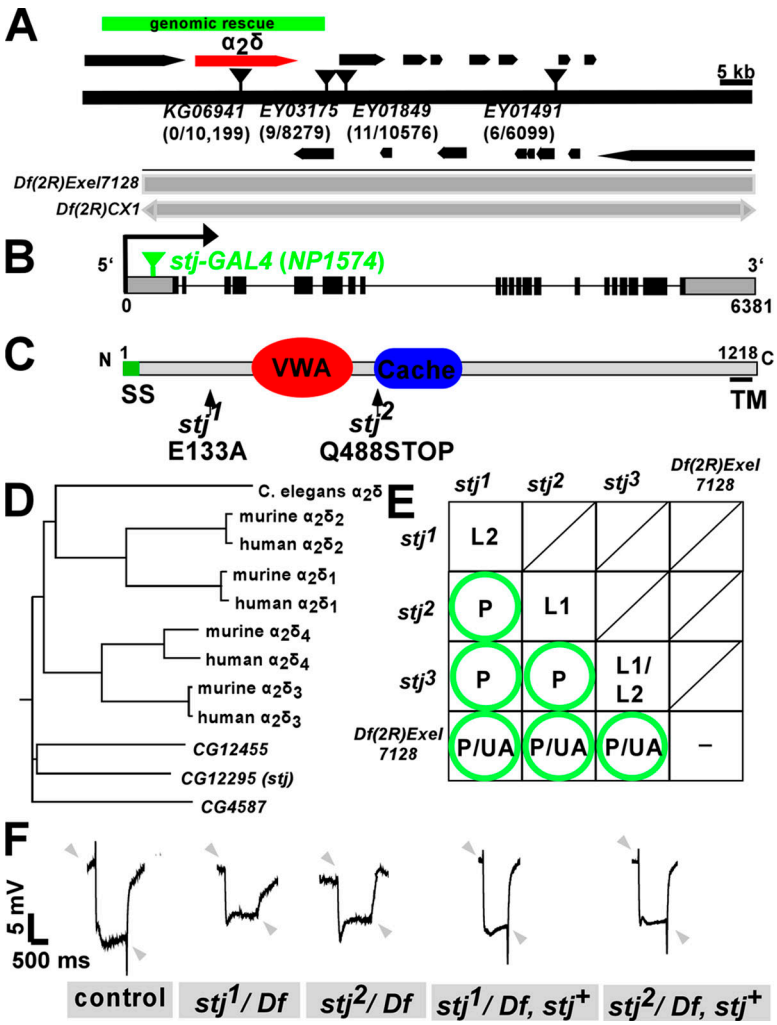

Figure 2. ***stj* encodes an accessory subunit of VGCCs.** (A) Mapping of *stj*. Recombination mapping using 4 *P* elements within an ~98-kbp region covered by a deficiency, *Df(2R)Exel7128* (gray bar), that fails to complement all *stj* alleles. *Df(2R)CX1* also fails to complement *stj* mutants (gray bar with arrows). The number of recombinants per flies scored is indicated below each *P* element (inverted triangles). Nearby genes are indicated (black bars). The region covered by a genomic rescue construct is indicated (green bar). (B) Exonic–intronic structure of *CG12295* (*stj*). The insertion position of *NP1574* (*stj-GAL4*; green inverted triangle) in the 5′ noncoding exon is designated. (C) Protein structure of Stj. Stj is 1,218 amino acids in length and contains a signal sequence (SS, green), a VWA domain (red), a Cache domain (blue), and a short C-terminal transmembrane region (TM, line). Mutations associated with the two characterized *stj* alleles are indicated. (D) $\alpha_2\delta$ phylogeny relating fly $\alpha_2\delta$s to nematode, mouse, and human homologues. (E) Lethal phase analysis of *stj* alleles. Extent of survival: L1, first instar; L2, second instar; P, pupae; UA, uncoordinated adult; –, not determined. Circles denote rescue to healthy adults by genomic construct. (F) Rescue of ERG defects by genomic *stj* construct. Arrowheads indicate the position of on–offs.

we used the *ey3.5FLP* system, which only drives FLP recombinase in presynaptic PRs (Chotard et al., 2005; Mehta et al., 2005). As shown in Fig. 1, the "on" transients remain absent, suggesting that the affected gene is required presynaptically (Fig. 1 B). Because failure to evoke a postsynaptic response may derive from impaired synaptic development or synaptic function, we performed electron microscopy to examine the lamina where R1-R6 PRs synapse with the postsynaptic monopolar cells to form cartridges with stereotyped organization (Kirschfeld, 1967; Clandinin and Zipursky, 2000). Similar to controls (Fig. 1, C and F), stj^1 (Fig. 1, D and G) and stj^2 (Fig. 1, E and H) *eyFLP* mutant cartridges predominantly possess six PR terminals per cartridge (Kirschfeld, 1967; Clandinin and Zipursky, 2000). We observe no other obvious morphological defects at these synapses. These data suggest that mutants have defective postsynaptic responses because of aberrant synaptic communication, not aberrant neuronal development.

stj encodes a *D. melanogaster* $\alpha_2\delta$ subunit

stj mutant third instar larvae are immobile with the exception of some head movements. Given the paralytic and ERG phenotypes, we sought to identify the gene affected in *stj* mutants. We used molecularly defined *P* elements (Zhai et al., 2003) to map *stj* to the 50C cytological interval of chromosome 2R. Deficiencies within the interval were then used to confirm and refine the mapping position. All three *stj* alleles failed to complement *Df(2R)CX1*[49C1-4;50C23-D2] and *Df(2R)Exel7128*[50C5;50C9], which spans a region <100 kbp (Fig. 2 A). Using *P* elements within the 50C5–50C9 interval, we performed fine mapping and found that a *P* element inserted in *CG12295*, *P*{*KG06941*} yielded zero recombinants out of ~10,000 flies (Fig. 2 A), which suggests that *CG12295* corresponds to *stj*. Sequencing of *CG12295* revealed a point mutation in stj^1, a Glu133Ala transition, altering a residue conserved in human and mouse homologues, and a nonsense mutation in stj^2, a Gln488STOP mutation (Figs. 2 C and S1, available at http://www.jcb.org/cgi/content/full/jcb.200712152/DC1). The stj^3 allele fails to complement the other two alleles and independently maps to the same locus as stj^1 and stj^2 but we were unable to define the molecular lesion. These data indicate that *stj* is *CG12295*.

CG12295 encodes an $\alpha_2\delta$ subunit of VGCCs. It contains a signal peptide, von Willebrand factor A (VWA) domain, Cache domain, and minimal transmembrane domain (Fig. 2 C). VWA domains are protein interaction domains common to integrins and other cell adhesion molecules (Whittaker and Hynes, 2002), whereas Cache domains, originally found in prokaryotic

chemotaxis receptors, are thought to mediate binding to small molecules such as amino acids (Anantharaman and Aravind, 2000). BLAST searches revealed three putative homologues of $\alpha_2\delta$ in the *D. melanogaster* genome compared with four in mammalian species. *CG12295* most closely resembles human $\alpha_2\delta_3$ (33% identical and 60% similar) and $\alpha_2\delta_4$ (31% identical and 59% similar; Figs. 2 D and S1). The VWA domain is particularly conserved, with 44% identity to $\alpha_2\delta_3$ and 48% identity to $\alpha_2\delta_4$. In addition, the Cache domain is 49–50% and 45% identical to vertebrate $\alpha_2\delta_3$ and $\alpha_2\delta_4$, respectively. $\alpha_2\delta_3$ and $\alpha_2\delta_4$ are less extensively characterized relative to other isoforms. Though no mutants currently exist for $\alpha_2\delta_3$, mutations in $\alpha_2\delta_4$ in mice and humans underlie PR dysfunction and progressive blindness (Wycisk et al., 2006a,b).

As homozygotes, the three *stj* alleles failed to survive beyond the early larval stages. However, when placed over *Df(2R)Exel7128* or in trans to one another, these larvae arrest as pupae and some emerge as uncoordinated adults, suggesting that these alleles may contain extraneous second site mutations that contribute to the homozygous lethality (Fig. 2 E). Of note, when over deficiency, both stj^1 and stj^3 alleles have similar lethal phases compared with the truncation mutant stj^2, indicating that both may constitute null or severe hypomorphic alleles.

To ascertain that the defects stem from loss of $\alpha_2\delta$, we introduced a 28.6-kbp genomic transgene in P[acman] (Venken et al., 2006) and neuronally expressed a full-length UAS-FLAG-*stj*-HA cDNA transgene in the mutants. The genomic construct rescued *stj/Df* and transheterozygote mutant combinations to adulthood (Fig. 2 E, circles). Note that some stj^1/Df and stj^2/Df animals eclose occasionally as adults but are severely uncoordinated (unpublished data) and unable to fly, whereas rescued adults walk and fly normally (unpublished data). In addition, the genomic transgene restored the physiological defects observed by ERG. Similar to *eyFLP* mutants (Fig. 1 A), stj^1/Df and stj^2/Df adult escapers also had reduced depolarization and loss of on–off transients. However, these ERG anomalies were corrected in the rescued adults (Fig. 2 F). The genomic *stj* transgene also restored on–off transients in $eyFLPstj^1$ and $eyFLPstj^2$ mutants (not depicted). Furthermore, when we used *C155-GAL4* to drive expression of UAS-FLAG-*stj*-HA panneuronally in stj^1/Df and stj^2/Df mutants, we also recovered viable adults. Thus, *stj* is required in the nervous system. Together, these findings show that *stj* is a crucial neuronal gene necessary for proper synaptic communication.

stj is expressed in neurons

To determine where *STJ* mRNA is expressed, we performed in situ hybridization on whole mount embryos. As shown in Fig. 3 A, the *STJ* message is expressed in the embryonic nervous system starting at stages 11 and 12 and is highly enriched in the brain and ventral nerve cord (VNC) in late stage embryos. A sense probe fails to label the embryonic brain (Fig. 3 B), indicating that the signal is specific to *STJ*. This is consistent with data showing that *STJ* mRNA is abundant in the brain and thoracico-abdominal ganglion of adult flies but is not detected in other adult tissues (www.FlyAtlas.org; Chintapalli et al., 2007). Thus, the *STJ* message is highly expressed in the *D. melanogaster* nervous system.

Given the paralysis in late larval stages, we turned to the third instar nervous system. We attempted to generate antibodies but were unsuccessful. However, we obtained an enhancer trap line (*NP1574*) that contains a *GAL4* driver (Kyoto Institute of Technology Drosophila Genetic Resource Center; Hayashi et al., 2002) within the 5′ untranslated region of *stj* (Fig. 2 B). Hence, in combination with a *UAS* reporter, *GAL4* expression of this enhancer trap may reveal the expression pattern of *stj*. In agreement with our in situ hybridization data, the *GAL4* driver is expressed in the brain and VNC in adults (Fig. 3 C) and larvae (Fig. 3, D–I′′), but is not present during early embryogenesis (not depicted). Therefore, we refer to *NP1574-GAL4* as *stj-GAL4*. Given the visual processing defects observed in *stj eyFLP* mutants (Fig. 1 A), we assessed *stj-GAL4*–driven GFP expression in the visual system. Cytoplasmic GFP is evident in PR axons and terminals and in the optic lobes of the adult brain, which is consistent with a role for *stj* in visual processing (Fig. 3 C). In third instar larvae, we detected *stj-GAL4*–driven GFP signal predominantly in a subset of cells in the VNC (Fig. 3 D) and salivary glands (not depicted). Here, GFP-positive cells are colabeled with the panneuronal marker Elav (Fig. 3 E; O'Neill et al., 1994) but not Repo (Fig. 3 F; Muhlig-Versen et al., 2005), a glial marker. However, *stj-GAL4* is expressed only in a subset of neurons within the VNC, some of which colocalize with Even-skipped (Fig. 3 G; Patel et al., 1994), a motor neuron marker. These motor neurons send axonal projections that form synapses outlined by the pre- and postsynaptic marker Dlg (Parnas et al., 2001) on body wall muscles 6/7 (Fig. 3, H and H′). Also, some GFP-positive neurons coincide with cell bodies labeled with anti-GABA (Fig. 3, I–I′′). GABA is synthesized by glutamate decarboxylase (GAD) found exclusively in inhibitory neurons, and, notably, GABA and GAD are present in cell bodies of the *D. melanogaster* nervous system (Buchner et al., 1988). Thus, *stj* is also present in a subpopulation of inhibitory interneurons. Therefore, *stj* is expressed in a discrete subset of neurons in the third instar larva, including motor neurons and inhibitory interneurons.

To examine the subcellular localization of Stj, we drove UAS-FLAG-*stj*-HA panneuronally using *C155-GAL4* in stj^1/Df mutants and labeled using antibodies to Syb (Fig. 3 J′), a synaptic marker, and HA (Fig. 3 J) to detect Stj. Unlike Cac, a presynaptic VGCC subunit that localizes to puncta corresponding to active zones (Kawasaki et al., 2004), Stj shows extensive colocalization with Syb and is distributed throughout the synapse (Fig. 3 J′′).

stj mutants are hyperexcitable

Disruption of vertebrate and invertebrate VGCCs have been shown to predispose organisms to epileptic events. Mouse mutants that affect various VGCC subunits, including α_1A (*tottering*), β_4 (*lethargic*), and $\alpha_2\delta_2$ (*ducky*), exhibit epileptic phenotypes (Burgess and Noebels, 1999). Furthermore, hypomorphic mutations in *cac* display seizure-like activity at elevated temperatures (Rieckhof et al., 2003), and *stj* (*CG12295*) expression is dynamically regulated in *D. melanogaster* seizure mutants (Guan et al., 2005). We therefore explored whether mutations in *stj* might also affect neuronal excitability by recording the endogenous

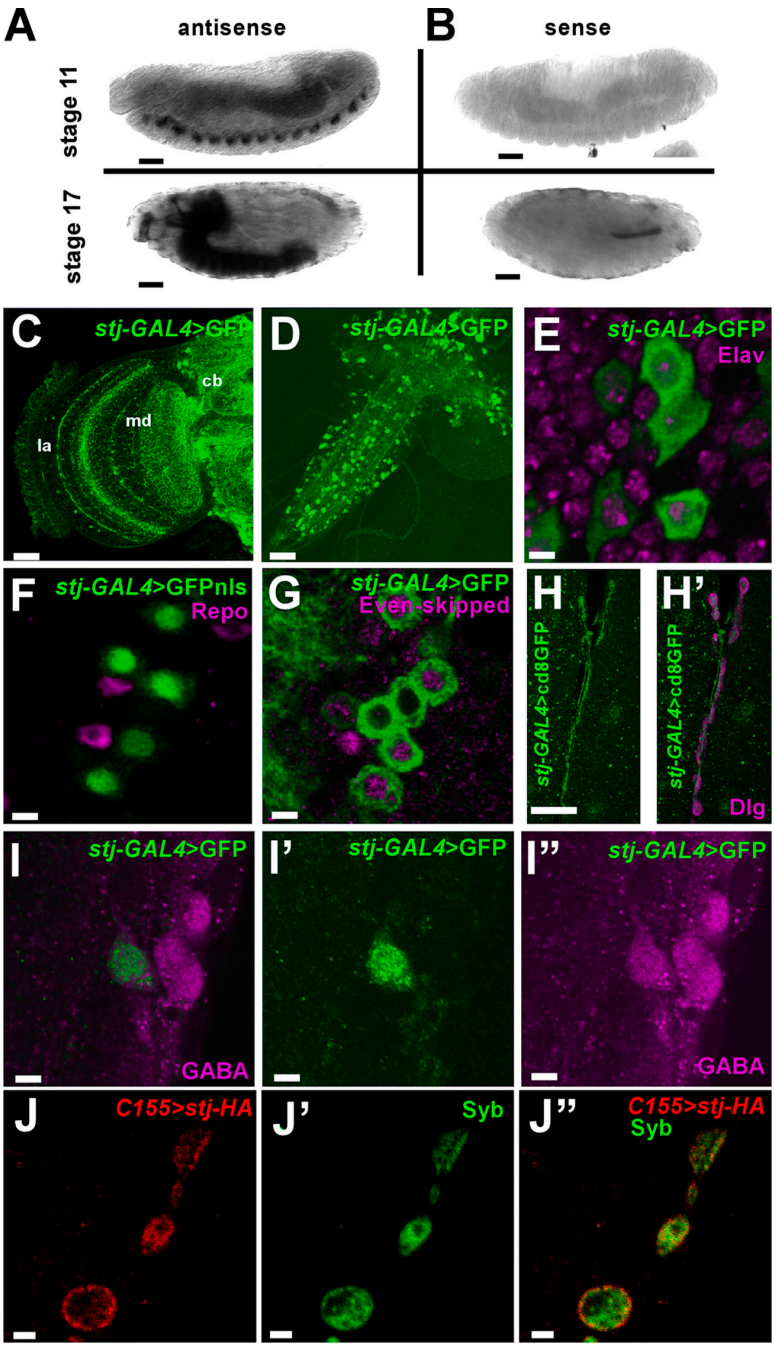

Figure 3. **Spatial expression of *stj* In situ hybridization on whole mount embryos.** (A) *STJ* message is enriched in the embryonic nervous system in stage 11 and 12 and stage 17 embryos. (B) A sense probe fails to label embryonic brain. Bars, 50 µm. (C–I'') *stj-GAL4* driven expression of *UAS-GFP* in adult (C) and larval brain (D–I''). (C) Adult brain with *stj-GAL4>UAS-GFP* enhanced using GFP antibody. la, lamina; md, medulla; cb, central brain. (D) Third instar larval brain with *stj-GAL4>UAS-GFP* enhanced using GFP antibody. (E and F) In larval brain, GFP expression is present in cells expressing the neuronal marker Elav (E, magenta) but is excluded from cells expressing the glial marker Repo (F, magenta). (G) *stj-GAL4>UAS-GFP* expression coincides with neurons expressing motorneuron marker Even-skipped (magenta). (H and H') GFP-positive motor neurons send projections that synapse upon muscles 6/7. Dlg demarcates the NMJ synapse and the synapse on muscles 6/7 is shown (H'). The green channel is shown separately in H. (I–I'') *stj-GAL4* drives GFP expression in neurons that costain with GABA antibody (I). Separated channels are shown in I' (GFP, green) and I'' (GABA, magenta). (J–J'') A tagged *stj* transgene driven in neurons (*C155-GAL4; stj^1/Df*; UAS-FLAG-*stj*-HA) labeled by an HA antibody (J) colocalizes with synaptic marker Syb (J'). A merged image is shown in J''. Bars: (A and B) 50 µm; (C) 30 µm; (D) 50 µm; (E–G) 4 µm; (H and H') 25 µm; (I–I'') 4 µm; (J–J'') 2 µm.

activity of the central pattern generator (CPG) for locomotion. We recorded from muscles 6/7 of dissected third instar larvae with intact VNCs at elevated temperature, a common paradigm for assessing seizure-like activity in *D. melanogaster* (Budnik et al., 1990; Rieckhof et al., 2003). Controls often exhibit rhythmic activity (Fig. 4, A and E). However, though burst events are relatively rare in *stj^1/Df* and *stj^2/Df* mutants, activity trains often last 30 s or longer (Fig. 4, B, C, and E). In addition, a genomic $\alpha_2\delta$ transgene restores rhythmic CPG activity in *stj^1/Df* and *stj^2/Df* mutants, indicating that these defects are specific to loss of *stj* (Fig. 4, D–E; and not depicted). Notably, mutant bursts are also lower in amplitude compared with the control (Fig. 4, B and C). The reduced amplitude of events is consistent with *stj* being expressed in motor neurons. Intriguingly, the loss of *stj* in a discrete subset of neurons, particularly GABA-ergic neurons, may contribute to neuronal hyperexcitability in these mutants by altering the balance of excitation and inhibition in the neuronal circuit subserving locomotion. Of note, GABA blockade has been shown to lead to seizure-like activity in flies (Stilwell et al., 2006). Together, this suggests that *stj* mutants show defects at both the network and synaptic levels.

stj mutants have defects in evoked neurotransmission

To assess neurotransmitter release at *stj* synapses, we performed additional electrophysiological recordings at the larval neuromuscular

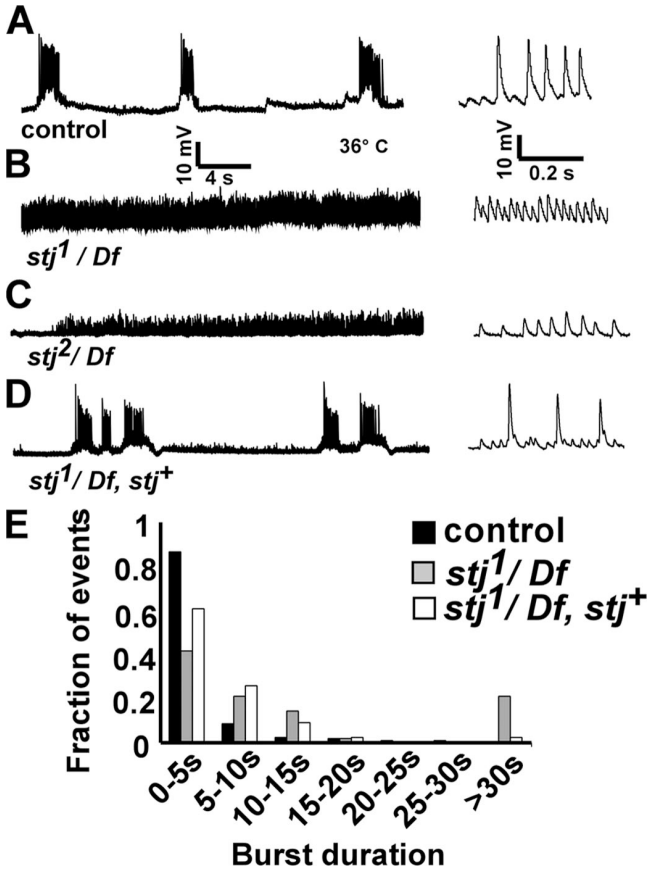

Figure 4. ***stj* mutants exhibit seizure-like activity.** (A–D) Muscle recordings of endogenous CPG activity performed at elevated temperature (36°C) with 1.5 mM Ca^{2+} for control (A; *y w; FRT42D*^{iso}), *stj*^{1}*/Df* (B; *y w eyFLP GMR-lacZ; FRT42D*^{iso} *stj*^{1}*/Df(2R)Exel7128*), *stj*^{2}*/Df* (C; *y w eyFLP GMR-lacZ; FRT42D*^{iso} *stj*^{2}*/Df(2R)Exel7128*), and rescued *stj*^{1}*/Df* (D; *y w eyFLP GMR-lacZ; FRT42D*^{iso} *stj*^{1}*/Df(2R)Exel7128, stj*$^{+}$) third instar larvae. (E) Histogram of burst duration. Events were analyzed from control (n = 274 from 8 larvae), *stj*^{1}*/Df* (n = 38 from six larvae), and rescued *stj*^{1}*/Df* (n = 135 from 10 larvae) by student's t test (*stj*^{1}*/Df*, $P < 0.01$).

junction (NMJ). Motor neurons were severed to prevent endogenous stimulation. We then stimulated control and mutant motor axons at 1 Hz in 1 mM Ca^{2+} and measured excitatory junctional potentials (EJPs) from the muscle. Compared with controls, all *stj* mutations over deficiency and in trans show a marked reduction in EJP amplitude (Fig. 5, A and B), revealing a severe defect in Ca^{2+}-regulated exocytosis. Notably, *stj* heterozygotes (*stj*/+) have EJP amplitudes similar to controls, indicating that there are no prominent dominant-negative effects associated with these mutations with respect to synaptic function (Fig. 5 B). Furthermore, when we introduce a genomic rescue construct in mutants over deficiency and in trans to one another, the reduced EJP amplitudes are restored (Fig. 5 B), which indicates that the loss of *stj* is solely responsible for the exocytic defect.

In addition to exocytic defects, a reduction in EJP amplitude may also reflect impairments in vesicular neurotransmitter loading or postsynaptic receptor function. To examine these possibilities, we measured spontaneous miniature EJPs (mEJPs) in *stj* mutants in 0.5 mM Ca^{2+} and 10 μM tetrodotoxin (TTX) to suppress evoked release. The mean mEJP amplitudes between control and mutants are not different (Fig. 5, C and D), nor are the distributions of mEJP event amplitudes (Fig. 5, F–H), which suggests that vesicle loading and postsynaptic receptor function are intact. In addition, we did not observe a difference in mEJP frequency between controls and *stj* mutants (Fig. 5 E). These results suggest that *stj* loss of function has predominant deleterious effects on exocytosis.

At synapses, Ca^{2+} is a key regulator of vesicle fusion and the amount of neurotransmitter released (Katz and Miledi, 1969). To explore the relationship between Ca^{2+} entry and evoked release at *stj* synapses, we measured EJPs, counting failures, at different extracellular Ca^{2+} concentrations from 0.1 to 1 mM Ca^{2+} ($[Ca^{2+}]_{ext}$). At every $[Ca^{2+}]_{ext}$ studied, EJP amplitudes in the mutant were reduced compared with controls (Fig. 5 I). To examine $[Ca^{2+}]$ sensitivity, we corrected for nonlinear summation of EJPs (Martin, 1955), determined quantal content, and generated a logarithmic plot of quantal content versus low $[Ca^{2+}]_{ext}$ (Fig. 5 J). Triggering of exocytosis relies upon cooperative binding of approximately three to four Ca^{2+} ions, which is reflected in the slope of the logarithmic plot (Dodge and Rahamimoff, 1967). We find that this slope is similar for both control (n = 3.1) and *stj* ^{1}*/Df* (n = 3.0), which suggests that cooperativity is not affected. However, the plot is right-shifted in *stj* ^{1}*/Df* (Fig. 5 J) and *stj* ^{2}*/Df* (not depicted), indicating a reduction in synaptic Ca^{2+} sensitivity.

We also examined control and *stj* mutant synapses for paired pulse facilitation, an enhancement of neurotransmitter release caused by elevation of residual Ca^{2+} in the nerve terminal (Zucker and Regehr, 2002). We applied two stimuli spaced 20, 50, and 100 ms apart and recorded EJPs in 1 mM Ca^{2+}. The extent of facilitation was expressed as the paired pulse ratio (PPR), EJP_2/EJP_1. When the pulse interval is 100 ms, there is no significant difference between the PPR in control and mutant animals. However, at pulse intervals of 50 and 20 ms (Fig. 5 K), *stj*^{1}*/Df* synapses exhibit increased facilitation compared with controls. Thus, the release probability at *stj* mutant synapses is reduced.

stj mutants exhibit a mild NMJ overgrowth but normal synaptic bouton ultrastructure

Synapse growth is regulated both by synaptic Ca^{2+} entry and activity. For instance, hypomorphic mutations in *cac*, the *D. melanogaster* α_1 subunit with similarity to N-, P/Q-, and R-type channels, have underdeveloped synapses (Rieckhof et al., 2003), whereas hyperexcitable *D. melanogaster* seizure mutants display synaptic overgrowth (Budnik et al., 1990). Because *stj* is a putative VGCC subunit and mutants display neuronal hyperexcitability, we assessed whether NMJ morphology might be altered by labeling control and mutant larvae with the pre- and postsynaptic marker Dlg (Parnas et al., 2001) and the presynaptic membrane marker Hrp (O'Neill et al., 1994). Relative to controls (Fig. 6, A and C), *stj* mutants (Fig. 6, B and C) exhibit a significant but mild synaptic overgrowth of the NMJ on muscles 6/7 in proportion to muscle size, reflected by a proportional increase in bouton number per muscle area (Fig. 6 D). This may be caused by the effect of hyperexcitability on synapse growth or a compensatory response to reduced synaptic transmission.

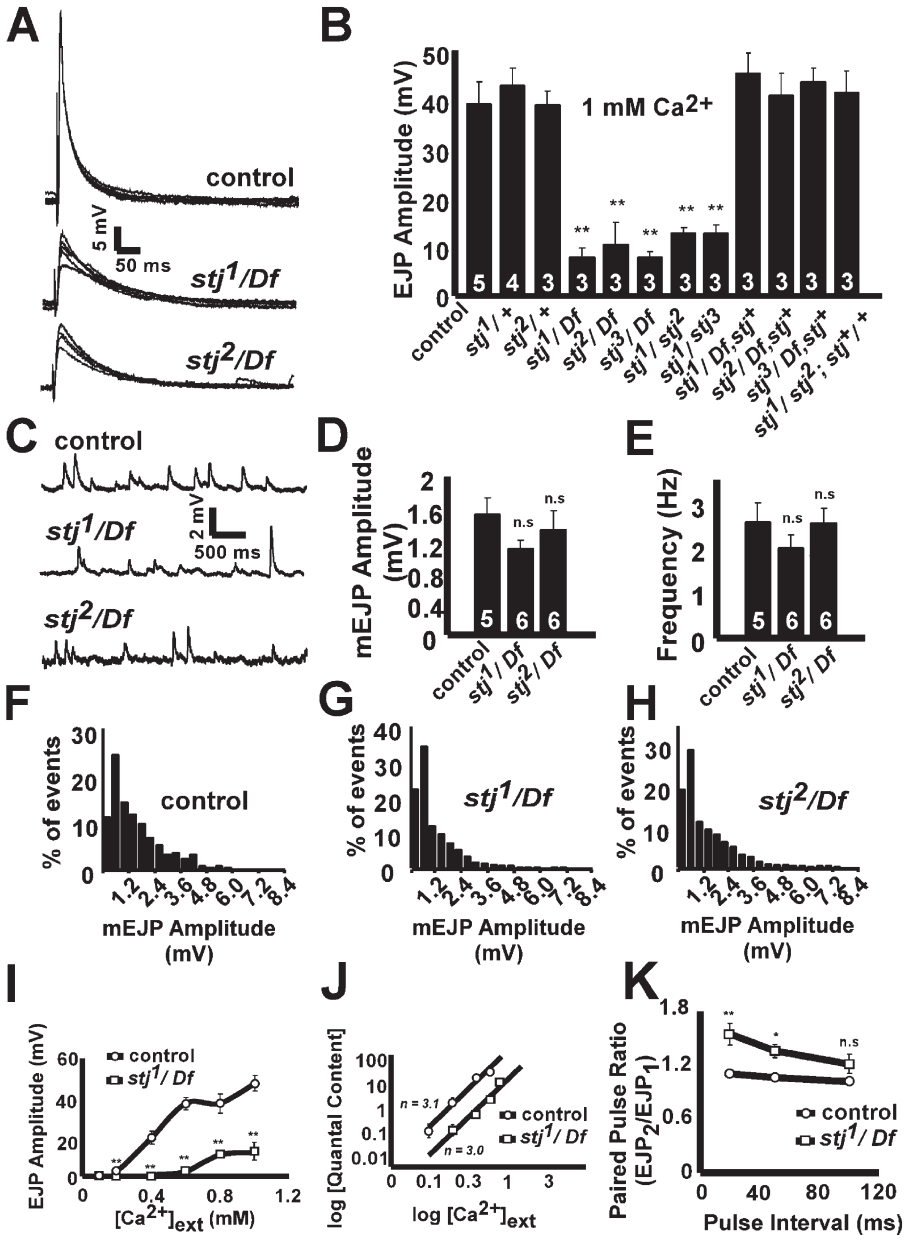

Figure 5. ***stj* mutants have severe defects in evoked neurotransmitter release.** (A) Sample EJPs recorded in 1 mM Ca^{2+} at 1 Hz in control, *stj*^{1}*/Df*, and *stj*^{2}*/Df* third instar NMJs. (B) Quantification of EJP amplitudes recorded at 1 Hz in 1 mM Ca^{2+}. Genotypes: control, 39 ± 5 mV; *stj*^{1}*/+* (*yw;FRT42D*^{iso} *stj*^{1}*/FRT42D*^{iso}), 43 ± 4 mV; *stj*^{2}*/+* (*y w; FRT42D*^{iso} *stj*^{2}*/FRT42D*^{iso}), 39 ± 3 mV; *stj*^{1}*/Df*, 8 ± 2 mV; *stj*^{2}*/Df*, 11 ± 5 mV; *stj*^{3}*/Df* (*y w eyFLP GMR-lacZ; FRT42D*^{iso} *stj*^{3}*/Df(2R)Exel7128*), 8 ± 1 mV; *stj*^{1}*/stj*^{2} (*y w eyFLP GMR-lacZ; FRT42D*^{iso} *stj*^{1}*/FRT42D*^{iso} *stj*^{2}), 13 ± 1 mV; *stj*^{1}*/stj*^{3} (*y w eyFLP GMR-lacZ; FRT42D*^{iso} *stj*^{1}*/FRT42D*^{iso} *stj*^{3}), 13 ± 2 mV; *stj*^{1}*/Df* rescue, 45 ± 4 mV; *stj*^{2}*/Df* rescue (*y w eyFLP GMR-lacZ;FRT42D*^{iso} *stj*^{2}*/Df(2R)Exel7128*), *stj*$^{+}$), 41 ± 5 mV; *stj*^{3}*/Df* rescue (*y w eyFLP GMR-lacZ; FRT42D*^{iso} *stj*^{3}*/Df(2R)Exel7128*), *stj*$^{+}$), 44 ± 3 mV; *stj*^{1}*/stj*^{2} rescue (*y w eyFLP GMR-lacZ; FRT-42D*^{iso} *stj*^{1}*/FRT42D*^{iso} *stj*^{2}*; stj*$^{+}$*/+*), 42 ± 4 mV. 60 EJP amplitudes were averaged per recording and the number of larvae tested is indicated in the bars. Error bars indicate SEM (student's *t* test; **, P < 0.01). (C) Sample mEJPs were recorded in 0.5 mM Ca^{2+} with 10 µM TTX to suppress evoked neuronal activity. Traces shown for control, *stj*^{1}*/Df*, and *stj*^{2}*/Df*. The mEJP amplitude (D), frequency (E), and mEJP amplitude distribution (F–H) of events larger than 0.4 mV are shown. The number of larvae analyzed is indicated in the bars (D and E). mEJP events were analyzed for control (*n* = 1,365), *stj*^{1}*/Df* (*n* = 1,109), and *stj*^{2}*/Df* (*n* = 1,215). The amplitude bin size was 0.2 mV. Error bars indicate SEM (student's *t* test; n.s., not significant). (I) EJPs amplitudes were measured at different $[Ca^{2+}]_{ext}$ (0.1, 0.2, 0.4, 0.6, 0.8, and 1 mM). Failures were included in the determination of EJP amplitudes to more accurately reflect synaptic release probabilities. Genotypes were control and *stj*^{1}*/Df*. Error bars indicate SEM; error bars smaller than data markers are not shown. (student's *t* test; **, P < 0.01). (J) Logarithmic plot of quantal content versus $[Ca^{2+}]_{ext}$. The slope of the line (*n*), indicated for control (*n* = 3.1) and *stj*^{1}*/Df* (*n* = 3.0), represents calcium cooperativity at these respective synapses. (K) Quantification of paired pulse ratio (PPR), EJP_2/EJP_1 for time intervals of 20 ms (control, PPR = 1.11 ± 0.03; *stj*^{1}*/Df*, PPR = 1.5 ± 0.1), 50 ms (control, PPR = 1.06 ± 0.02; *stj*^{1}*/Df*, PPR = 1.36 ± 0.07), and 100 ms (control, PPR = 1.018 ± 0.007; *stj*^{1}*/Df*, PPR = 1.21 ± 0.1). Error bars indicate SEM (student's *t* test; n.s., not significant; *, P < 0.05; **, P < 0.01).

To more closely examine single boutons, ultrastructural analyses were performed on control (Fig. 6, E and G) and mutant (Fig. 6, F and H) boutons. However, these studies revealed no differences in vesicle density (Fig. 6 I), synaptic length (Fig. 6 J), active zone density (Fig. 6 K), number of active zone–associated vesicles (Fig. 6 L), or vesicle size (Fig. 6, M and N). Notably, the subsynaptic reticulum (SSR) surrounding the boutons appears more disordered in mutant boutons. However, even when SSR is almost entirely absent, as in *dpix* mutants (Parnas et al., 2001), synaptic function is only mildly affected. Thus, our SSR defect is not likely to contribute to the impaired synaptic release in *stj* mutants. These data indicate that though NMJ synapses are slightly overgrown in *stj* mutants, most aspects of bouton architecture are intact.

Cac is reduced at *stj* synapses

Given the similarity of *stj* and *cac* phenotypes (Smith et al., 1998; Rieckhof et al., 2003), we determined whether Cac is properly localized in *stj* mutants. When expressed solely in neurons, *cacEGFP* (Kawasaki et al., 2004) rescues the embryonic lethality as well as synaptic function of *cac* null mutants and localizes to synaptic active zones. Therefore, we expressed *cacEGFP* in control and mutant neurons using *C155-GAL4*. We visualized *C155-GAL4*–driven expression of CacEGFP (green) at control and *stj* mutant NMJs (Fig. 7, A and D) and costained with Bruchpilot (Brp; Fig. 7, A′ and D′, magenta), an active zone marker (Wucherpfennig et al., 2003), and Dlg to outline synapses (not depicted). Because native CacEGFP fluorescence is weak, we amplified the signal using tyramide enhancement

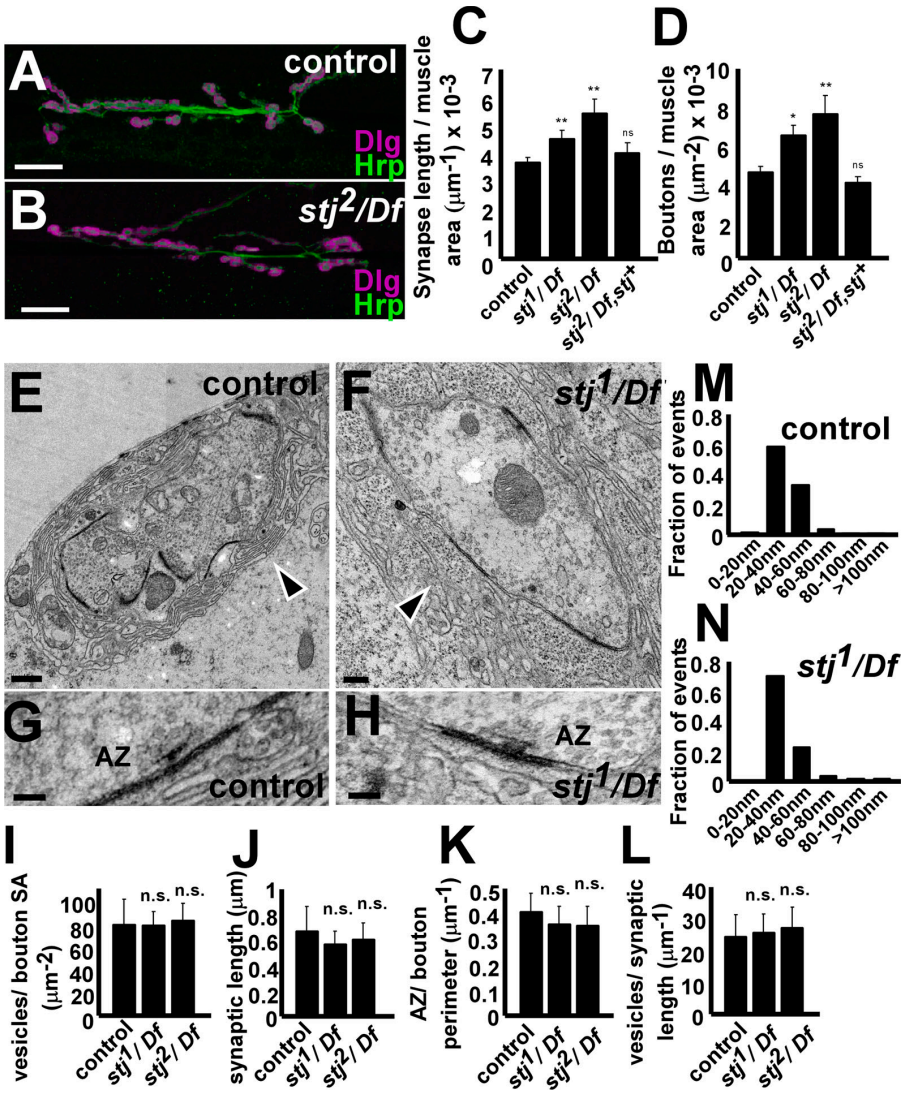

Figure 6. ***stj* mutant synapses exhibit NMJ overgrowth but have normal bouton ultrastructure.** Third instar NMJ synapses of muscles 6/7 in control (A) and stj^2/Df (B) stained for Dlg (magenta) and Hrp (green). Bar, 25 µm. (C and D) Quantification of NMJ synapse length (C; controls, 0.0036 ± 0.0002 $µm^{-1}$; stj^1/Df, 0.0044 ± 0.0003 $µm^{-1}$; stj^2/Df, 0.0053 ± 0.0005 $µm^{-1}$; stj^2/Df, stj^+, 0.0038 ± 0.0004 $µm^{-1}$) and bouton number (D; controls, 0.00045 ± 0.00003 $µm^{-2}$; stj^1/Df, 0.00064 ± 0.00005 $µm^{-2}$; stj^2/Df, 0.0008 ± 0.0001 $µm^{-2}$; stj^2/Df, stj^+, 0.0004 ± 0.00003 $µm^{-2}$) normalized to muscle area. Number of animals analyzed: controls, $n = 21$; stj^1/Df, $n = 13$; stj^2/Df, $n = 10$; stj^2/Df, stj^+, $n = 7$. Error bars indicate SEM (student's *t* test; *, $P < 0.05$, **, $P < 0.01$). (E–H) TEM of NMJ boutons in control (E and G) and stj^2/Df (F and H). Synaptic features such as vesicles, active zones (AZ), and the SSR (arrowheads) are readily observed. Quantification of bouton parameters in control, stj^1/Df, and stj^2/Df animals including vesicle density (I), synaptic length (J), AZ density (K), AZ-associated vesicles (within a 100-nm perimeter of the AZ; L), and vesicle size (M and N) revealed no significant differences. Number of vesicles analyzed from: control, $n = 425$; and stj^1/Df, $n = 475$. However, the SSR appears disordered in stj^1/Df (not depicted) and stj^2/Df (F, arrowhead) boutons. Cross sections from at least 10 boutons from three animals were examined for each genotype. Error bars indicate SEM (student's *t* test; n.s., not significant). Bars: (A and B) 25 µm; (E) 0.5 µm; (F) 0.2 µm; (G and H) 100 nm.

(see Materials and methods). At *C155-GAL4/+; UAS-cacEGFP/+* NMJs, we often observed CacEGFP puncta that are adjacent to Brp (Fig. 7, A–A′′) despite some diffusion of the enhanced CacEGFP signal. However, in *C155-GAL4/+;* stj^1/Df, *UAS-cacEGFP* synapses, although we also observed colocalization between CacEGFP and Brp (Fig. 7, D–D′′), the CacEGFP signal intensity was significantly reduced compared with controls (Fig. 7 G). To determine the background signal associated with tyramide enhancement, we simultaneously labeled Canton-S larvae. We observed a weak, nonspecific synaptic signal associated with the tyramide reaction (Fig. S2, available at http://www.jcb.org/cgi/content/full/jcb.200712152/DC1) but never observed punctate signal in Canton-S larvae, which suggests that the CacEGFP signal we detected in *C155-GAL4/+; UAS-cacEGFP/+* and *C155-GAL4/+;* stj^1/Df, *UAS-cacEGFP* larvae is specific. Moreover, we quantified the density and signal intensity of Brp at control and mutant synapses overexpressing CacEGFP and found that although signal intensity is mildly increased in the mutants (Fig. 7 H), Brp puncta density (Fig. 7 I) is not different. Thus, active zones remain stable even when synaptic Ca^{2+} channels are markedly reduced. Together, this suggests that CacEGFP can properly traffic to active zones independently of *stj* but requires *stj* to ensure appropriate levels of Cac at the synapse.

To determine whether the reduction in synaptic CacEGFP might stem from global mistrafficking or reduced stability of Cac in *stj* mutants, we also looked at the VNC (Fig. 7, B and E) and axonal projections (Fig. 7, C and F) of control and mutant larvae overexpressing *cacEGFP*. We found that CacEGFP was distributed similarly within cell bodies throughout the VNC in control (Fig. 7 B) and mutant (Fig. 7 E) animals. Furthermore, the signal intensities of CacEGFP within the VNC of control and mutant animals are not different (Fig. 7 J). In addition, levels of CacEGFP are similar within axonal projections (Fig. 7 K). Hence, the data indicate that *stj* is not crucial for the global stabilization or axonal transport of Cac but rather plays a more discrete role in stabilizing Cac locally at synapses.

Neuronal overexpression of *cac* partially rescues *stj* phenotypes

Interestingly, when we expressed *cac*EGFP panneuronally in stj^1/Df and stj^2/Df mutant backgrounds, we observed a partial rescue

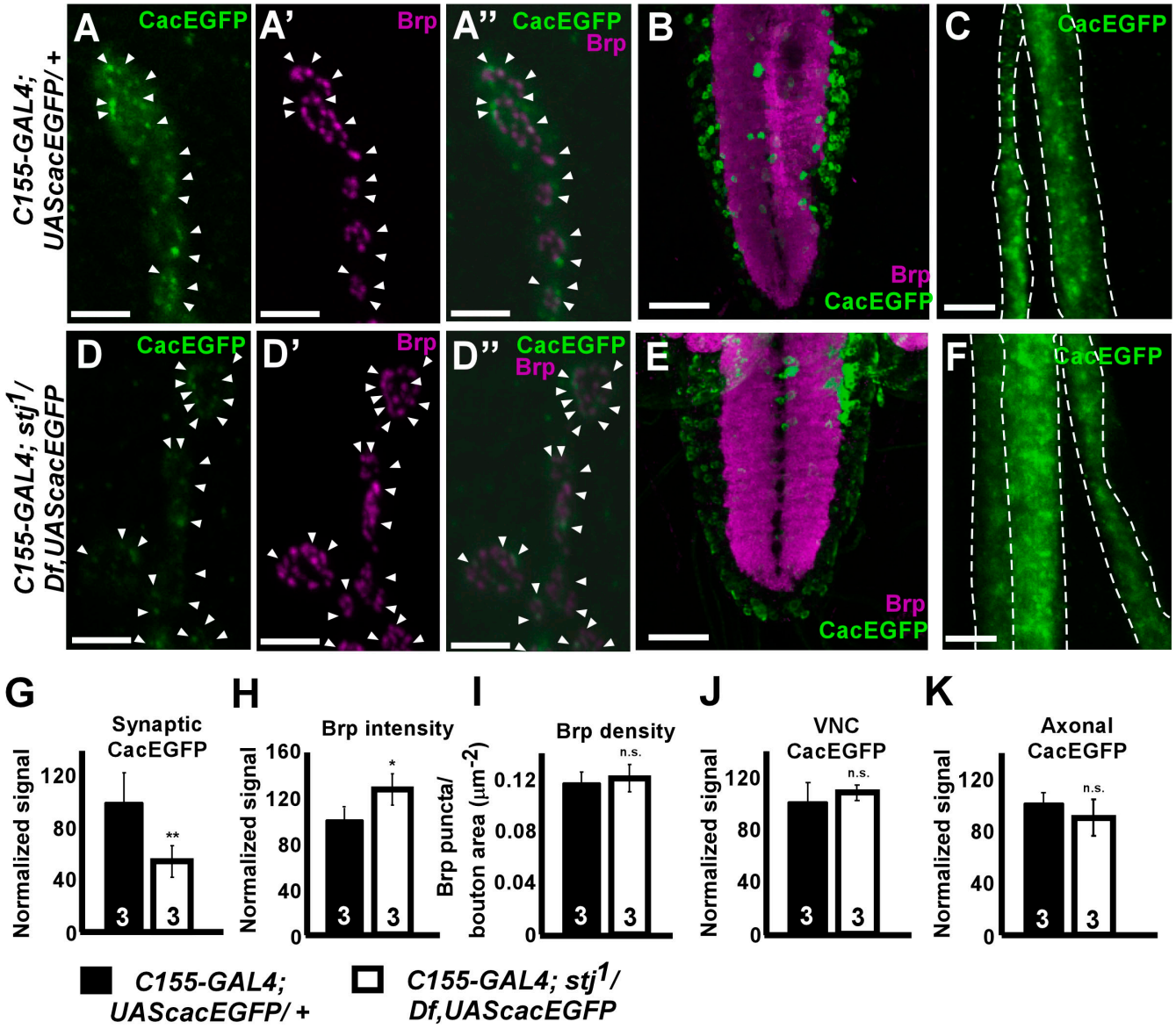

Figure 7. **Cac is mislocalized in *stj* mutants.** (A and D) NMJ synapses from C155-GAL4; UAScacEGFP/+ (C155-GAL4; FRT42D^{iso}/UAS-cacEGFP; A–A'') and C155-GAL4; stj^1/Df, UAScacEGFP (C155-GAL4; FRT42D^{iso} stj^1/Df(2R)Exel7128, UAS-cacEGFP; D–D'') larvae labeled with tyramide-enhanced CacEGFP (A and D, green) and Brp (A' and D', magenta). Merged images are shown (A'' and D''). Brightness of green channel (CacEGFP) was enhanced in merged images to emphasize colocalization. Arrowheads denote CacEGFP puncta coinciding with Brp. (B and E) Larval VNC from C155-GAL4; UAScacEGFP/+ (B) and C155-GAL4; stj^1/Df, UAScacEGFP (E) colabeled with tyramide-enhanced CacEGFP (green) and Brp (magenta). CacEGFP-labeled axonal segments from C155-GAL4; UAScacEGFP/+ (C) and C155-GAL4; stj^1/Df, UAScacEGFP (F). Broken lines delineate axonal bundles. (G–K) Quantification of CacEGFP (G) and Brp (H) signal intensity at NMJs. (I) Brp puncta density at NMJs. (J and K) Quantification of CacEGFP signal intensity within VNC (J) and axonal projections (K). Number of larvae analyzed is indicated in the bars. For NMJ quantifications, at least 14 NMJs from three animals were analyzed. Error bars indicate SEM (student's *t* test; n.s., not significant; *, P < 0.05; **, P < 0.01). Bars: (A and D) 4 μm; (B and E) 50 μm; (C and F) 6 μm.

of viability (Fig. 8 A). However, no viable flies were obtained in the absence of *cac*EGFP or when *cac*EGFP was expressed postsynaptically in the muscle using the *MHC-GAL4* driver (Fig. 8 A), indicating that the rescue activity of *cac*EGFP is dependent on its neuronal expression. In addition, we recorded ERGs from *C155-GAL4; stj^1/Df, UAS-cacEGFP* and *C155-GAL4; stj^2/Df, UAS-cacEGFP* adult flies and found that they possess on–off transients (Fig. 8 B, arrowheads), unlike *stj^2/Df* adult escapers (Fig. 8 B) and *stj eyFLP* mutants (Fig. 1). Also, *C155-GAL4; stj^1/Df, UAS-cacEGFP* and *C155-GAL4; stj^2/Df, UAS-cacEGFP* third instar larvae displayed greater mobility than homozygous *stj* mutant larvae, which barely move (unpublished data). To determine whether neuronal expression of *cac*EGFP affects the function of *stj* mutant NMJs, we recorded EJPs in 1 mM Ca^{2+} at 1 Hz from *C155-GAL4; UAS-cacEGFP/+*, *C155-GAL4; stj^1/Df, UAS-cacEGFP*, and *C155-GAL4; stj^2/Df, UAS-cacEGFP* larvae (Fig. 8, C and D). Neuronal expression of *cacEGFP* alone did not alter the EJP amplitude compared with controls (Fig. 8 D). However, although *C155-GAL4; stj^1/Df, UAS-cacEGFP* and *C155-GAL4; stj^2/Df, UAS-cacEGFP* larvae have reduced EJP amplitudes compared with controls, the response is increased relative to *stj^1/Df* and *stj^2/Df* (Fig. 8, C and D). In addition, we

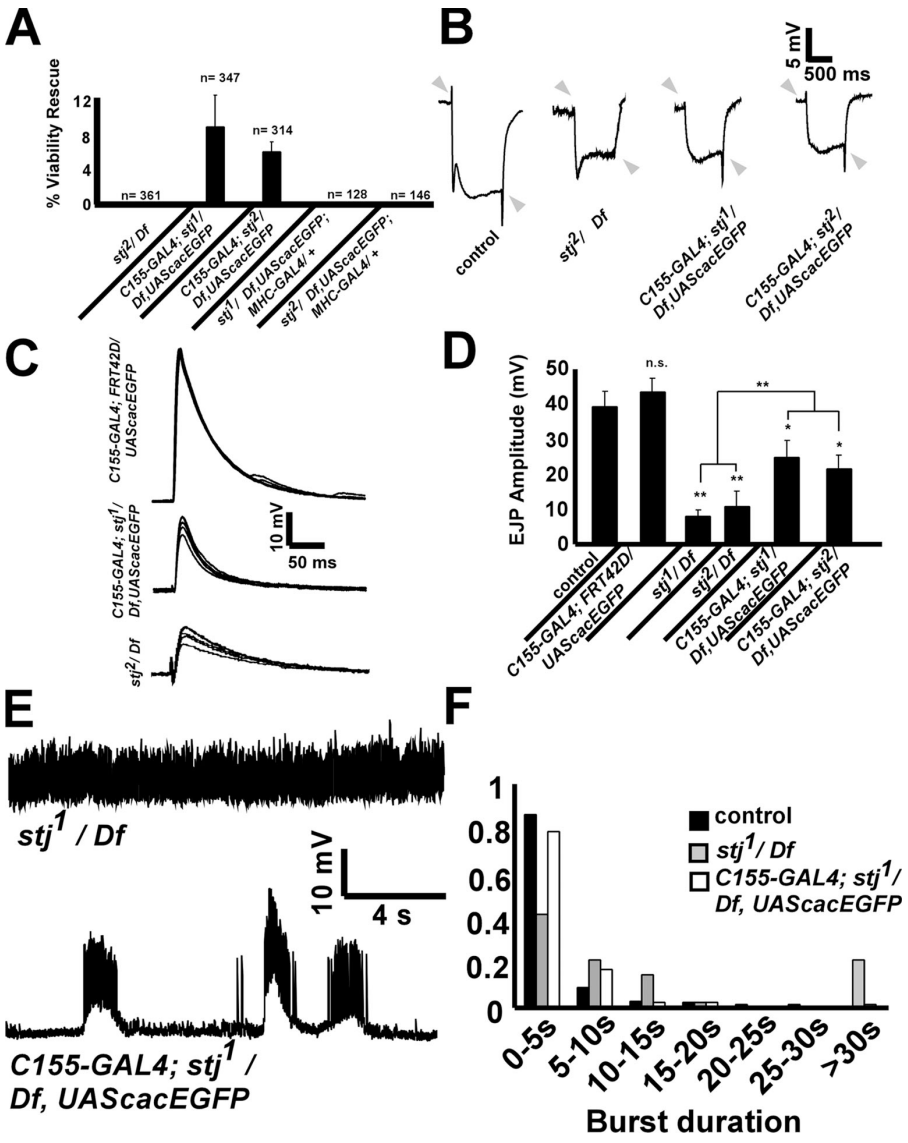

Figure 8. ***cac* overexpression partially rescues *stj* phenotypes.** (A) Viability rescue of *stj* mutants by neuronal expression of *cacEGFP*. Percentages were calculated from the number of viable flies out of the expected number of flies based on a Mendelian ratio. *n*, number of flies counted from three to eight separate crosses. Genotypes scored: stj^2/Df, *C155-GAL4;* stj^1/Df, *UAScacEGFP, C155-GAL4;* stj^2/Df, *UAScacEGFP, FRT42D*^{iso} stj^1*/Df-UAS-cacEGFP; MHC-GAL4/+*, and *FRT42D*^{iso} stj^2*/Df-UAS-cacEGFP; MHC-GAL4/+*. (B) ERGs recorded from *C155-GAL4;* stj^1/Df, *UAScacEGFP* and *C155-GAL4;* stj^2/Df, *UAScacEGFP* flies have on–offs (arrowheads) similar to control ERGs. stj^2/Df escapers lack on–offs. (C) Sample EJPs recorded in 1 mM Ca^{2+} at 1 Hz in *C155-GAL4; UAScacEGFP/+, C155-GAL4;* stj^1/Df, *UAScacEGFP* and stj^2/Df. (D) Quantification of EJP amplitudes from control (39 ± 2 mV) *C155-GAL4; UAScacEGFP/+* (44 ± 4 mV), stj^1/Df (8 ± 2 mV), stj^2/Df (11 ± 5 mV), *C155-GAL4;* stj^1/Df, *UAScacEGFP* (25 ± 5 mV) and *C155-GAL4;* stj^2/Df, *UAScacEGFP* (21 ± 4 mV). Error bars indicate SEM (student's *t* test; n.s., not significant; *, $P < 0.05$; **, $P < 0.01$). (E) Sample recordings of endogenous CPG activity at 36°C in 1.5 mM Ca^{2+} for stj^1/Df and *C155-GAL4;* stj^1/Df, *UAS-cacEGFP*. (F) Histogram of burst duration. Number of events analyzed from: control, *n* = 274 from eight animals; stj^1/Df, *n* = 38 from six larvae; and *C155-GAL4;* stj^1/Df, *UAS-cacEGFP*, *n* = 109 from four larvae (student's *t* test; stj^1/Df, $P < 0.01$).

investigated the effect of *cacEGFP* overexpression on the hyperexcitability observed in *stj* mutants by recording endogenous CPG activity from *C155-GAL4;* stj^1/Df, *UAS-cacEGFP*. Unlike stj^1/Df, mutants overexpressing *cacEGFP* rarely exhibit activity bursts lasting 30 s or more (Fig. 8, E and F). Thus, panneuronal expression of *cacEGFP* can partially rescue the viability and functional defects associated with *stj* loss of function. Together, this further indicates that *stj* genetically interacts with *cac*.

Discussion

Neuronal communication between synapses involves regulated exocytosis of neurotransmitter at presynaptic sites, a process triggered by regulated influx of Ca^{2+} through VGCCs (Smith and Augustine, 1988; Catterall, 1998; Robitaille et al., 1990). VGCCs are thought to be comprised of a protein complex consisting of a pore-forming α_1 subunit along with several accessory subunits including β, γ, and $\alpha_2\delta$ (Takahashi et al., 1987; Tanabe et al., 1987). Here, we describe the isolation and characterization of *D. melanogaster* $\alpha_2\delta$ mutants named *stj*. *stj* mutants display seizure-like activity and a severe reduction in synaptic release. Our findings indicate that these defects stem from a failure to properly stabilize Cac, a presynaptic α_1 pore subunit, at synapses.

Although four $\alpha_2\delta$ homologues exist in vertebrates, only three $\alpha_2\delta$ subunits are encoded in flies. The three *D. melanogaster* $\alpha_2\delta$ homologues are most similar to mammalian $\alpha_2\delta_3$ and $\alpha_2\delta_4$, which are the least characterized in vertebrates. Though mutants of vertebrate $\alpha_2\delta_1$ and $\alpha_2\delta_3$ have not yet been described, mutations in $\alpha_2\delta_4$ impair retinal function, resulting in a slowly progressing cone dystrophy in patients that leads to blindness (Wycisk et al., 2006a,b). Notably, PR function is disrupted in *cac* mutants (Smith et al., 1998), and we also find that *stj* mutants have abnormal ERGs, suggesting a conserved role for VGCCs in retinal signaling. Consistent with this finding, another study on the *D. melanogaster* $\alpha_2\delta$ subunit (i.e., *stj* and *d*$\alpha_2\delta$) published while this manuscript was in submission also reported aberrant PR signaling (Dickman et al., 2008). Notably, we find that PR morphology in the visual system is intact, suggesting that the defect is functional, not developmental, in nature.

Further insight into the in vivo role of $\alpha_2\delta$ has been garnered through work on a spontaneous mouse mutant of $\alpha_2\delta_2$ known as *ducky*. The three alleles of *ducky*, *ducky* (Barclay et al., 2001), *ducky*^{2J} (Donato et al., 2006), and *Cacna2d2*^{entla} (Brill et al., 2004), exhibit spike-wave seizures reminiscent of absence epilepsy and are ataxic. Similarly, we also find that *stj* mutants have altered neuronal excitability and surmise that this may be caused by a selective loss of *stj* in a subset of neurons, possibly inhibitory interneurons. Consistent with this possibility, blockade of GABA receptors in *D. melanogaster* larvae has been shown to predispose to neuronal hyperactivity (Stilwell et al., 2006).

Five functionally distinct VGCC α_1 subtypes encoded by 10 different genes are expressed in mammalian excitable tissues, L-, N-, P/Q-, R-, and T-types (Catterall, 2000). However, within the *D. melanogaster* genome, there are only four genes that encode α_1 subunits representing homologues of vertebrate N-, P/Q-, and R-type (*cac*, also known as *dmca1A*; Smith et al., 1996), L-type (*dmca1D*; Zheng et al., 1995), and T-type (*dmca1T*) channels (*CG15899*; http://flybase.bio.indiana.edu/) and an invertebrate-specific α_1 subunit (*dmalpha1U*, also known as *narrow abdomen* and *halothane resistance*; Nash et al., 2002). However, we focused on *cac* for the following reasons. First, mutations in *dmalpha1U* are viable and predominantly affect diurnal locomotor activity patterns but exhibit no other obvious neurological deficits (Nash et al., 2002). Second, *dmca1T* has not been characterized in the fly and no phenotypic analysis is available. Third, *dmca1D* is thought to primarily underlie muscle Ca^{2+} currents (Zheng et al., 1995; Ren et al., 1998). Although *dmca1D* transcripts are expressed in the brain, the function of *dmca1D* in the nervous system has not been established (Zheng et al., 1995). However, *cac* mutants display a marked reduction in synaptic release, similar to what is observed when *stj* is lost, and is likely the primary α_1 subunit involved in neurotransmission in flies (Smith et al., 1996; Kawasaki et al., 2000). In addition, *cac* mutants have ERG (Smith et al., 1998) and seizure (Rieckhof et al., 2003) phenotypes similar to *stj* mutants. The synaptic defects in *cac* mutants can be corrected by neuronal expression of *cac* cDNA, which suggests a requirement for this gene in the nervous system (Kawasaki et al., 2004). Consistent with this data, *stj* is predominantly expressed and required in the nervous system, as demonstrated by our ability to rescue the mutants with a neuronally driven *stj* transgene and in situ hybridization studies. Together, the neuronal localization and phenotypic similarities suggest that *cac* is a likely target for *stj* function.

Work in heterologous expression systems has demonstrated that $\alpha_2\delta$ subunits can increase Ca^{2+} current amplitudes approximately threefold by increasing the expression of α_1 on the membrane (Singer et al., 1991; Felix et al., 1997; Klugbauer et al., 1999; Gao et al., 2000; Canti et al., 2005). In addition, *ducky* mutant Purkinje cells exhibit a ~35% reduction in P-type Ca^{2+} currents despite no changes in unitary Ca^{2+} currents (Barclay et al., 2001). However, evidence of channel mislocalization in *ducky* mice has not been demonstrated and the mechanism by which $\alpha_2\delta_2$ loss leads to the defects in *ducky* mice remains unclear. Similar to Dickman et al. (2008), we observe a severe reduction in EJP amplitude at *stj* mutant NMJ synapses. We find that this impairment is likely caused by a reduction in the highly Ca^{2+}-dependent release probability because we observed increased facilitation at *stj* synapses and a rightward shift in the Ca^{2+} dependence of neurotransmitter release. The alternate study partially attributes the reduction in synaptic release to a reduced number of active zones, suggested by a decreased mEJP frequency and a reduction in Brp labeling (Dickman et al., 2008). However, we do not observe a loss of active zones in *stj* mutants. Notably, they compared their mutants to Canton-S to assess Brp labeling, whereas a different control (w^{118}) was used for electrophysiological analyses. Because it was not reported whether these defects could be corrected by $d\alpha_2\delta$ transgene expression, we cannot exclude that some of the defects are due to genetic background.

However, we do find that CacEGFP is dramatically reduced at mutant synapses when expressed panneuronally, demonstrating a direct role for an $\alpha_2\delta$ subunit in regulating the synaptic levels of an α_1 subunit in vivo, a finding also corroborated by Dickman et al. (2008). Interestingly, although CacEGFP is reduced at *stj* mutant synapses, it properly localizes to active zones, suggesting that the synaptic targeting of Cac does not depend solely on *stj* and requires other factors. In addition, we do not observe differences in CacEGFP distribution or signal in the VNC or axonal projections, indicating that the global stability and axonal transport of Cac are not affected by *stj* loss of function. Hence, *stj* most likely plays a discrete role in the synaptic stabilization of Cac.

Interestingly, we also find that neuronal overexpression of *cac* can partially rescue the viability and electrophysiological phenotypes observed in *stj* mutants, providing further evidence that they interact. In contrast, although Dickman et al. (2008) found that *cacEGFP* overexpression improves the survival of their mutants, they did not observe an improvement in EJP amplitude when *cacEGFP* is overexpressed in the mutants. To measure *cacEGFP* rescue activity at the NMJ, Dickman et al. (2008) performed electrophysiological recordings in 0.3 mM Ca^{2+}, whereas our studies were done in 1 mM Ca^{2+}. It is possible that at 0.3 mM Ca^{2+}, the mutants, which display a right-shift in Ca^{2+} sensitivity, are operating in a subcooperative regimen where the ameliorative effects of *cacEGFP* overexpression are masked. Notably, the ERG, hyperexcitability, and NMJ synaptic release phenotypes are improved in our mutants with neuronal *cac* overexpression. Hence, *stj* is required for the proper function and localization of Cac but this defect can be partially overcome with *cac* overexpression.

In summary, we have isolated novel mutations in *stj*, a neuronal *D. melanogaster* $\alpha_2\delta$ subunit. Our studies define a predominant role for a *D. melanogaster* $\alpha_2\delta$ in regulating neuronal excitability and neurotransmitter release by specifically stabilizing *cac*, a presynaptic VGCC α_1 subunit, at synapses. This work should facilitate further studies to illuminate the role of $\alpha_2\delta$ as a therapeutic target and modulator of VGCC function.

Materials and methods

D. melanogaster strains and genetics

The isolation of 118 mutants on chromosome 2R, including *stj*^{1}, *stj*^{2}, *and stj*^{3}, has been described previously (Verstreken et al., 2002). The control genotype was *y w; P{ry*$^{+}$ *neoFRT}42D*^{isogenized} (FRT42D^{iso}). Flies with visual

systems homozygous for *stj* were *y w eyFLP GMR-lacZ; FRT42D^{iso}stj/FRT-42D^{iso}, P{w$^+$ ry$^+$}47A l(2)cl-R11^1*. Mapping of *stj* is described in Fig. 2 A. *P* element stocks and *Df(2R)CX1* (indicated in Fig. 2 A) were obtained from the Bloomington Drosophila Stock Center (Brizuela et al., 1994; Bellen et al., 2004; Parks et al., 2004). *Df(2R)Exel7128* was obtained from the Exelixis stock collection (Thibault et al., 2004). *stj^1*, *stj^2*, *stj^3*, and *Df(2R)Exel7128* were maintained over *CyO; Kr-GAL4 UAS-GFP* and mutant animals were cultured on grape juice plates with yeast paste. *NP1574-GAL4* was obtained from the Kyoto Institute of Technology Drosophila Genetic Resource Center (Hayashi et al., 2002) and was crossed to *UAS-GFP*, *UAS-GFP$_{nls}$*, or *UAS-mCD8GFP* as indicated (Fig. 3). *UAS-cac*EGFP flies were obtained from R. Ordway (Pennsylvania State University, University Park, PA; Kawasaki et al., 2004). We analyzed *C155-GAL4/+; FRT42D^{iso}/UAS-cac*EGFP, *C155-GAL4/+; stj^1/Df(2R)Exel7128, UAS-cac*EGFP, and *C155-GAL4/+; stj^2/Df(2R)Exel7128, UAS-cacEGFP*.

Molecular biology

28 kb of genomic DNA harboring *CG12295* (*stj*) was recovered from BAC16G12 (BACPAC Resources Center) by gap repair in P[acman] ApR F-2-5 (provided by K. Venken, Baylor College of Medicine, Houston, TX; Venken et al., 2006). We cloned a 501-bp left and 448-bp right homology arm separated by a BamHI site in P[acman]. The vector was digested with BamHI and transformed into recombination competent mini-λ-Tet DH10B bacteria containing BAC16G12. Gap-repaired vectors containing the genomic *stj* sequence were selected by AMP and verified by sequencing and restriction analysis. To generate the *UAS-FLAG-stj-HA* transgene, we PCR amplified the coding region of *stj* from cDNA clone SD07723 (Drosophila Gene Collection 1; Rubin, 2000) by primers CG12295–BglII–F (GAAGATCTAATGGCCTGGTCCCGTCTCCTG) and *stj*-HA–XbaI–R (TTTCTAGATCGCGTAGTCGGGGACGTCGTAGGGGTATCTAGACAGCCAACGACTCAGTATGTG), which includes the corresponding sequence of the HA tag, and subcloned it into the BglII and XbaI sites of the pUAST-Flag vector (Yao and Sun, 2005).

In situ hybridization

A 1,489-bp sequence corresponding to nucleotides 1–1,489 of *stj* was amplified from cDNA clone SD07723 (Drosophila Gene Collection 1; Rubin, 2000) and cloned into the pBluescript KS (+) vector containing flanking T7 and T3 promoter elements using BglII and XhoI restriction sites. Probe synthesis, embryo fixation, and in situ hybridization was performed as described previously (Lecuyer et al., 2007).

Immunohistochemistry

Larvae and adult flies raised at 22°C were dissected in modified HL3 solution (110 mM NaCl, 5 mM KCl, 10 mM $NaHCO_3$, 5 mM Hepes, 30 mM sucrose, 5 mM trehalose, and 10 mM $MgCl_2$, pH 7.2) and fixed in 3.7% formaldehyde. Stainings were performed using standard protocols (Bellen et al., 2004). Samples were mounted in Vectashield (Vector Laboratories). Images were captured at room temperature using a confocal microscope (LSM 510; Carl Zeiss, Inc.) with LSM5 software (Carl Zeiss, Inc.) using the following objectives: Plan Apochromat 63× 1.4 NA, Plan Neofluar 40× 1.3 NA, and Plan Neofluar 16× 0.5 NA (all from Carl Zeiss, Inc.). Images were processed with Amira 2.2 (TGS), Photoshop 7.0 (Adobe), and ImageJ. Primary antibodies specific to these antigens were used at the following dilutions: Brp, 1:20 (mouse, nc82; Developmental Studies Hybridoma Bank; Wucherpfennig et al., 2003); Dlg, 1:50 (mouse, 4F3; Developmental Studies Hybridoma Bank; Parnas et al., 2001); Dlg, 1:200 (rabbit, provided by K. Choi, Baylor College of Medicine, Houston, TX); Elav, 1:50 (mouse, 9F8A9; Developmental Studies Hybridoma Bank; O'Neill et al., 1994); Even-skipped, 1:10 (mouse, 2B8; Developmental Studies Hybridoma Bank; Patel et al., 1994); HA, 1: 500 (mouse, 16B12; Covance); Hrp, 1:200 (rabbit; Jackson ImmunoResearch Laboratories); GFP, 1:200 (rabbit; Invitrogen); GFP, 1:10,000 (chicken; Abcam); Repo, 1:10 (mouse, 8D12; Developmental Studies Hybridoma Bank; Muhlig-Versen et al., 2005); and Syb, 1: 200 (rat; Wu et al., 1999). Secondary antibodies tagged with Alexa 488 (Invitrogen), Cy3, Cy5, or Hrp (Jackson ImmunoResearch Laboratories) were used at 1:200.

We detected CacEGFP signals by performing tyramide signal amplification (PerkinElmer). In brief, after a 10-min fixation with 3.7% formaldehyde, we washed dissected third instar larvae three times with PBT (PBS with 0.2% Triton X-100) and incubated preparations in 1% hydrogen peroxide for 1 h. After several washes, samples were blocked in 10% normal goat serum (NGS) for 1 h. Samples were incubated overnight with chicken anti-GFP. The preparations were washed with PBT, incubated in 10% NGS for 1 h, and allowed to incubate with Hrp-conjugated anti–chicken. After several washes, samples were incubated with tyramide in amplification buffer (PerkinElmer) for 30 min. Samples were then washed in PBT, blocked in 10% NGS, and incubated with additional primary antibodies for 2 h. After several washes and a blocking treatment, secondary antibodies were applied for 2 h. After a final wash, preparations were mounted in Vectashield and imaged.

Electrophysiology

ERGs were recorded as described previously (Fabian-Fine et al., 2003; Verstreken et al., 2003). Third instar larval electrophysiological recordings were performed as described previously (Verstreken et al., 2002). Larvae were maintained in modified HL3 (110 mM NaCl, 5 mM KCl, 10 mM $NaHCO_3$, 5 mM Hepes, 30 mM sucrose, 5 mM trehalose, and 10 mM $MgCl_2$, pH 7.2) and recordings were performed in various extracellular [Ca^{2+}] as indicated. In CPG recordings, larval motor axons were left intact and endogenous neural activity was recorded from muscles 6/7 at 36°C with the temperature controlled as described previously (Koh et al., 2004). To measure EJPs, we stimulated cut motor neurons and recorded from muscles 6/7/12/13. Quantal content was estimated by including failures and correcting for nonlinear summation of EJPs (Martin, 1955). Cooperativity coefficients were then assessed by determining the slope of log-transformed measurements for quantal content for Ca^{2+} concentrations of 0.1–0.8 mM. mEJPs were recorded in the presence of 0.5 mM extracellular Ca^{2+} and 10 μM TTX (Sigma-Aldrich). EJPs and mEJPs were analyzed using pClamp6 and Mini Analysis Program (Synaptosoft) software, respectively.

Transmission electron microscopy (TEM)

TEM of PRs was performed as described previously (Hiesinger et al., 2006). At least 15 cartridges from three animals were examined. TEM of NMJ boutons was performed as described previously (Verstreken et al., 2002). Analysis was performed on ∼15 boutons from at least three larvae. Images were analyzed using ImageJ.

Online supplemental material

Fig. S1 shows a protein sequence alignment comparing *stj* with murine and human $\alpha_2\delta_{1-4}$ proteins and indicates the residues affected in *stj^1* and *stj^2* alleles. Fig. S2 shows that tyramide enhancement in non-*cacEGFP*–expressing controls leads to a nonspecific synaptic signal that is diffuse, not punctate, as is the case when *cacEGFP* is present. Online supplemental material is available at http://www.jcb.org/cgi/content/full/jcb.200712152/DC1.

We thank Koen Venken for sharing the P[acman] vector before publication. We thank Richard Ordway, the Bloomington Drosophila Stock Center, and Kyoto Drosophila Genetic Resource Center for reagents. We thank Amir Fayazzudin, Yong Qi Lin, other members of the Bellen laboratory, and Christian Rosenmund for discussions. We thank Karen Schulze, Bryan Michael Thomas, and Kyong-Mi Um for their help. We are grateful to Richard Atkinson and Claire Haueter for microscopy expertise and Yuchun He for injections to make transgenic lines.

Confocal microscopy was supported by the Baylor College of Medicine Mental Retardation and Developmental Disabilities Research Center. C.V. Ly is supported by an Ruth L. Kirschstein National Research Service Award from the National Institute of Neurological Disorders and Stroke (grant F30NS056520). H.J. Bellen is an Howard Hughes Medical Institute investigator.

Submitted: 26 December 2007
Accepted: 10 March 2008

References

Anantharaman, V., and L. Aravind. 2000. Cache - a signaling domain common to animal Ca(2+)-channel subunits and a class of prokaryotic chemotaxis receptors. *Trends Biochem. Sci.* 25:535–537.

Bahls, F.H., R. Lartius, L.E. Trudeau, R.T. Doyle, Y. Fang, D. Witcher, K. Campbell, and P.G. Haydon. 1998. Contact-dependent regulation of N-type calcium channel subunits during synaptogenesis. *J. Neurobiol.* 35:198–208.

Barclay, J., N. Balaguero, M. Mione, S.L. Ackerman, V.A. Letts, J. Brodbeck, C. Canti, A. Meir, K.M. Page, K. Kusumi, et al. 2001. Ducky mouse phenotype of epilepsy and ataxia is associated with mutations in the Cacna2d2 gene and decreased calcium channel current in cerebellar Purkinje cells. *J. Neurosci.* 21:6095–6104.

Bellen, H.J., R.W. Levis, G. Liao, Y. He, J.W. Carlson, G. Tsang, M. Evans-Holm, P.R. Hiesinger, K.L. Schulze, G.M. Rubin, et al. 2004. The BDGP

gene disruption project: single transposon insertions associated with 40% of *Drosophila* genes. *Genetics.* 167:761–781.

Benzer, S. 1967. Behavioral nutants of *Drosophila* isolated by countercurrent distribution. *Proc. Natl. Acad. Sci. USA.* 58:1112–1119.

Brill, J., R. Klocke, D. Paul, D. Boison, N. Gouder, N. Klugbauer, F. Hofmann, C.M. Becker, and K. Becker. 2004. entla, a novel epileptic and ataxic Cacna2d2 mutant of the mouse. *J. Biol. Chem.* 279:7322–7330.

Brizuela, B.J., L. Elfring, J. Ballard, J.W. Tamkun, and J.A. Kennison. 1994. Genetic analysis of the brahma gene of *Drosophila melanogaster* and polytene chromosome subdivisions 72AB. *Genetics.* 137:803–813.

Buchner, E., R. Bader, S. Buchner, J. Cox, P.C. Emson, E. Flory, C.W. Heizmann, S. Hemm, A. Hofbauer, and W.H. Oertel. 1988. Cell-specific immunoprobes for the brain of normal and mutant *Drosophila melanogaster*. I. Wildtype visual system. *Cell Tissue Res.* 253:357–370.

Budnik, V., Y. Zhong, and C.F. Wu. 1990. Morphological plasticity of motor axons in *Drosophila* mutants with altered excitability. *J. Neurosci.* 10:3754–3768.

Burgess, D.L., and J.L. Noebels. 1999. Single gene defects in mice: the role of voltage-dependent calcium channels in absence models. *Epilepsy Res.* 36:111–122.

Canti, C., M. Nieto-Rostro, I. Foucault, F. Heblich, J. Wratten, M.W. Richards, J. Hendrich, L. Douglas, K.M. Page, A. Davies, and A.C. Dolphin. 2005. The metal-ion-dependent adhesion site in the Von Willebrand factor-A domain of alpha2delta subunits is key to trafficking voltage-gated Ca2+ channels. *Proc. Natl. Acad. Sci. USA.* 102:11230–11235.

Catterall, W.A. 1998. Structure and function of neuronal Ca2+ channels and their role in neurotransmitter release. *Cell Calcium.* 24:307–323.

Catterall, W.A. 2000. Structure and regulation of voltage-gated Ca2+ channels. *Annu. Rev. Cell Dev. Biol.* 16:521–555.

Chintapalli, V.R., J. Wang, and J.A. Dow. 2007. Using FlyAtlas to identify better *Drosophila melanogaster* models of human disease. *Nat. Genet.* 39:715–720.

Chotard, C., W. Leung, and I. Salecker. 2005. glial cells missing and gcm2 cell autonomously regulate both glial and neuronal development in the visual system of *Drosophila*. *Neuron.* 48:237–251.

Clandinin, T.R., and S.L. Zipursky. 2000. Afferent growth cone interactions control synaptic specificity in the *Drosophila* visual system. *Neuron.* 28:427–436.

De Jongh, K.S., C. Warner, and W.A. Catterall. 1990. Subunits of purified calcium channels. Alpha 2 and delta are encoded by the same gene. *J. Biol. Chem.* 265:14738–14741.

Dickman, D.K., P.T. Kurshan, and T.L. Schwarz. 2008. Mutations in a *Drosophila* alpha2delta voltage-gated calcium channel subunit reveal a crucial synaptic function. *J. Neurosci.* 28:31–38.

Dodge, F.A. Jr., and R. Rahamimoff. 1967. On the relationship between calcium concentration and the amplitude of the end-plate potential. *J. Physiol.* 189:90P–92P.

Donato, R., K.M. Page, D. Koch, M. Nieto-Rostro, I. Foucault, A. Davies, T. Wilkinson, M. Rees, F.A. Edwards, and A.C. Dolphin. 2006. The ducky(2J) mutation in Cacna2d2 results in reduced spontaneous Purkinje cell activity and altered gene expression. *J. Neurosci.* 26:12576–12586.

Ellis, S.B., M.E. Williams, N.R. Ways, R. Brenner, A.H. Sharp, A.T. Leung, K.P. Campbell, E. McKenna, W.J. Koch, A. Hui, et al. 1988. Sequence and expression of mRNAs encoding the alpha 1 and alpha 2 subunits of a DHP-sensitive calcium channel. *Science.* 241:1661–1664.

Fabian-Fine, R., P. Verstreken, P.R. Hiesinger, J.A. Horne, R. Kostyleva, Y. Zhou, H.J. Bellen, and I.A. Meinertzhagen. 2003. Endophilin promotes a late step in endocytosis at glial invaginations in *Drosophila* photoreceptor terminals. *J. Neurosci.* 23:10732–10744.

Felix, R., C.A. Gurnett, M. De Waard, and K.P. Campbell. 1997. Dissection of functional domains of the voltage-dependent Ca2+ channel alpha2delta subunit. *J. Neurosci.* 17:6884–6891.

Gao, B., Y. Sekido, A. Maximov, M. Saad, E. Forgacs, F. Latif, M.H. Wei, M. Lerman, J.H. Lee, E. Perez-Reyes, et al. 2000. Functional properties of a new voltage-dependent calcium channel alpha(2)delta auxiliary subunit gene (CACNA2D2). *J. Biol. Chem.* 275:12237–12242.

Gee, N.S., J.P. Brown, V.U. Dissanayake, J. Offord, R. Thurlow, and G.N. Woodruff. 1996. The novel anticonvulsant drug, gabapentin (Neurontin), binds to the alpha2delta subunit of a calcium channel. *J. Biol. Chem.* 271:5768–5776.

Guan, Z., S. Saraswati, B. Adolfsen, and J.T. Littleton. 2005. Genome-wide transcriptional changes associated with enhanced activity in the *Drosophila* nervous system. *Neuron.* 48:91–107.

Gurnett, C.A., M. De Waard, and K.P. Campbell. 1996. Dual function of the voltage-dependent Ca2+ channel alpha 2 delta subunit in current stimulation and subunit interaction. *Neuron.* 16:431–440.

Hayashi, S., K. Ito, Y. Sado, M. Taniguchi, A. Akimoto, H. Takeuchi, T. Aigaki, F. Matsuzaki, H. Nakagoshi, T. Tanimura, et al. 2002. GETDB, a database compiling expression patterns and molecular locations of a collection of Gal4 enhancer traps. *Genesis.* 34:58–61.

Herlitze, S., M. Xie, J. Han, A. Hummer, K.V. Melnik-Martinez, R.L. Moreno, and M.D. Mark. 2003. Targeting mechanisms of high voltage-activated Ca2+ channels. *J. Bioenerg. Biomembr.* 35:621–637.

Hiesinger, P.R., R.G. Zhai, Y. Zhou, T.W. Koh, S.Q. Mehta, K.L. Schulze, Y. Cao, P. Verstreken, T.R. Clandinin, K.F. Fischbach, et al. 2006. Activity-independent prespecification of synaptic partners in the visual map of *Drosophila*. *Curr. Biol.* 16:1835–1843.

Jay, S.D., A.H. Sharp, S.D. Kahl, T.S. Vedvick, M.M. Harpold, and K.P. Campbell. 1991. Structural characterization of the dihydropyridine-sensitive calcium channel alpha 2-subunit and the associated delta peptides. *J. Biol. Chem.* 266:3287–3293.

Katz, B., and R. Miledi. 1969. Spontaneous and evoked activity of motor nerve endings in calcium Ringer. *J. Physiol.* 203:689–706.

Kawasaki, F., R. Felling, and R.W. Ordway. 2000. A temperature-sensitive paralytic mutant defines a primary synaptic calcium channel in *Drosophila*. *J. Neurosci.* 20:4885–4889.

Kawasaki, F., B. Zou, X. Xu, and R.W. Ordway. 2004. Active zone localization of presynaptic calcium channels encoded by the cacophony locus of *Drosophila*. *J. Neurosci.* 24:282–285.

Kirschfeld, K. 1967. The projection of the optical environment on the screen of the rhabdomere in the compound eye of the *Musca*. [In German.] *Exp. Brain Res.* 3:248–270

Klugbauer, N., L. Lacinova, E. Marais, M. Hobom, and F. Hofmann. 1999. Molecular diversity of the calcium channel alpha2delta subunit. *J. Neurosci.* 19:684–691.

Koh, T.W., P. Verstreken, and H.J. Bellen. 2004. Dap160/intersectin acts as a stabilizing scaffold required for synaptic development and vesicle endocytosis. *Neuron.* 43:193–205.

Komuro, H., and P. Rakic. 1998. Orchestration of neuronal migration by activity of ion channels, neurotransmitter receptors, and intracellular Ca2+ fluctuations. *J. Neurobiol.* 37:110–130.

Lecuyer, E., H. Yoshida, N. Parthasarathy, C. Alm, T. Babak, T. Cerovina, T.R. Hughes, P. Tomancak, and H.M. Krause. 2007. Global analysis of mRNA localization reveals a prominent role in organizing cellular architecture and function. *Cell.* 131:174–187.

Martin, A.R. 1955. A further study of the statistical composition on the end-plate potential. *J. Physiol.* 130:114–122.

Mehta, S.Q., P.R. Hiesinger, S. Beronja, R.G. Zhai, K.L. Schulze, P. Verstreken, Y. Cao, Y. Zhou, U. Tepass, M.C. Crair, and H.J. Bellen. 2005. Mutations in *Drosophila* sec15 reveal a function in neuronal targeting for a subset of exocyst components. *Neuron.* 46:219–232.

Mikami, A., K. Imoto, T. Tanabe, T. Niidome, Y. Mori, H. Takeshima, S. Narumiya, and S. Numa. 1989. Primary structure and functional expression of the cardiac dihydropyridine-sensitive calcium channel. *Nature.* 340:230–233.

Muhlig-Versen, M., A.B. da Cruz, J.A. Tschape, M. Moser, R. Buttner, K. Athenstaedt, P. Glynn, and D. Kretzschmar. 2005. Loss of Swiss cheese/neuropathy target esterase activity causes disruption of phosphatidylcholine homeostasis and neuronal and glial death in adult *Drosophila*. *J. Neurosci.* 25:2865–2873.

Nash, H.A., R.L. Scott, B.C. Lear, and R. Allada. 2002. An unusual cation channel mediates photic control of locomotion in *Drosophila*. *Curr. Biol.* 12:2152–2158.

Newsome, T.P., B. Asling, and B.J. Dickson. 2000. Analysis of *Drosophila* photoreceptor axon guidance in eye-specific mosaics. *Development.* 127:851–860.

O'Neill, E.M., I. Rebay, R. Tjian, and G.M. Rubin. 1994. The activities of two Ets-related transcription factors required for *Drosophila* eye development are modulated by the Ras/MAPK pathway. *Cell.* 78:137–147.

Pak, W.L., J. Grossfield, and N.V. White. 1969. Nonphototactic mutants in a study of vision of *Drosophila*. *Nature.* 222:351–354.

Parks, A.L., K.R. Cook, M. Belvin, N.A. Dompe, R. Fawcett, K. Huppert, L.R. Tan, C.G. Winter, K.P. Bogart, J.E. Deal, et al. 2004. Systematic generation of high-resolution deletion coverage of the *Drosophila melanogaster* genome. *Nat. Genet.* 36:288–292.

Parnas, D., A.P. Haghighi, R.D. Fetter, S.W. Kim, and C.S. Goodman. 2001. Regulation of postsynaptic structure and protein localization by the Rho-type guanine nucleotide exchange factor dPix. *Neuron.* 32:415–424.

Patel, N.H., B.G. Condron, and K. Zinn. 1994. Pair-rule expression patterns of even-skipped are found in both short- and long-germ beetles. *Nature.* 367:429–434.

Pietrobon, D. 2005. Function and dysfunction of synaptic calcium channels: insights from mouse models. *Curr. Opin. Neurobiol.* 15:257–265.

Qin, N., R. Olcese, E. Stefani, and L. Birnbaumer. 1998. Modulation of human neuronal alpha 1E-type calcium channel by alpha 2 delta-subunit. *Am. J. Physiol.* 274:C1324–C1331.

Ren, D., H. Xu, D.F. Eberl, M. Chopra, and L.M. Hall. 1998. A mutation affecting dihydropyridine-sensitive current levels and activation kinetics in *Drosophila* muscle and mammalian heart calcium channels. *J. Neurosci.* 18:2335–2341.

Rieckhof, G.E., M. Yoshihara, Z. Guan, and J.T. Littleton. 2003. Presynaptic N-type calcium channels regulate synaptic growth. *J. Biol. Chem.* 278:41099–41108.

Robitaille, R., E.M. Adler, and M.P. Charlton. 1990. Strategic location of calcium channels at transmitter release sites of frog neuromuscular synapses. *Neuron.* 5:773–779.

Rubin, G.M. 2000. Biological annotation of the *Drosophila* genome sequence. *Novartis Found. Symp.* 229:79–82 (discussion 82–3).

Sandoval, A., N. Oviedo, A. Andrade, and R. Felix. 2004. Glycosylation of asparagines 136 and 184 is necessary for the alpha2delta subunit-mediated regulation of voltage-gated Ca2+ channels. *FEBS Lett.* 576:21–26.

Singer, D., M. Biel, I. Lotan, V. Flockerzi, F. Hofmann, and N. Dascal. 1991. The roles of the subunits in the function of the calcium channel. *Science.* 253:1553–1557.

Smith, S.J., and G.J. Augustine. 1988. Calcium ions, active zones and synaptic transmitter release. *Trends Neurosci.* 11:458–464.

Smith, L.A., X. Wang, A.A. Peixoto, E.K. Neumann, L.M. Hall, and J.C. Hall. 1996. A *Drosophila* calcium channel alpha1 subunit gene maps to a genetic locus associated with behavioral and visual defects. *J. Neurosci.* 16:7868–7879.

Smith, L.A., A.A. Peixoto, E.M. Kramer, A. Villella, and J.C. Hall. 1998. Courtship and visual defects of cacophony mutants reveal functional complexity of a calcium-channel alpha1 subunit in *Drosophila*. *Genetics.* 149:1407–1426.

Stilwell, G.E., S. Saraswati, J.T. Littleton, and S.W. Chouinard. 2006. Development of a *Drosophila* seizure model for in vivo high-throughput drug screening. *Eur. J. Neurosci.* 24:2211–2222.

Stowers, R.S., and T.L. Schwarz. 1999. A genetic method for generating *Drosophila* eyes composed exclusively of mitotic clones of a single genotype. *Genetics.* 152:1631–1639.

Takahashi, M., M.J. Seagar, J.F. Jones, B.F. Reber, and W.A. Catterall. 1987. Subunit structure of dihydropyridine-sensitive calcium channels from skeletal muscle. *Proc. Natl. Acad. Sci. USA.* 84:5478–5482.

Tanabe, T., H. Takeshima, A. Mikami, V. Flockerzi, H. Takahashi, K. Kangawa, M. Kojima, H. Matsuo, T. Hirose, and S. Numa. 1987. Primary structure of the receptor for calcium channel blockers from skeletal muscle. *Nature.* 328:313–318.

Thibault, S.T., M.A. Singer, W.Y. Miyazaki, B. Milash, N.A. Dompe, C.M. Singh, R. Buchholz, M. Demsky, R. Fawcett, H.L. Francis-Lang, et al. 2004. A complementary transposon tool kit for *Drosophila melanogaster* using P and piggyBac. *Nat. Genet.* 36:283–287.

Venken, K.J., Y. He, R.A. Hoskins, and H.J. Bellen. 2006. P[acman]: a BAC transgenic platform for targeted insertion of large DNA fragments in *D. melanogaster*. *Science.* 314:1747–1751.

Verstreken, P., O. Kjaerulff, T.E. Lloyd, R. Atkinson, Y. Zhou, I.A. Meinertzhagen, and H.J. Bellen. 2002. Endophilin mutations block clathrin-mediated endocytosis but not neurotransmitter release. *Cell.* 109:101–112.

Verstreken, P., T.W. Koh, K.L. Schulze, R.G. Zhai, P.R. Hiesinger, Y. Zhou, S.Q. Mehta, Y. Cao, J. Roos, and H.J. Bellen. 2003. Synaptojanin is recruited by endophilin to promote synaptic vesicle uncoating. *Neuron.* 40:733–748.

Verstreken, P., C.V. Ly, K.J. Venken, T.W. Koh, Y. Zhou, and H.J. Bellen. 2005. Synaptic mitochondria are critical for mobilization of reserve pool vesicles at *Drosophila* neuromuscular junctions. *Neuron.* 47:365–378.

Whittaker, C.A., and R.O. Hynes. 2002. Distribution and evolution of von Willebrand/integrin A domains: widely dispersed domains with roles in cell adhesion and elsewhere. *Mol. Biol. Cell.* 13:3369–3387.

Wu, M.N., T. Fergestad, T.E. Lloyd, Y. He, K. Broadie, and H.J. Bellen. 1999. Syntaxin 1A interacts with multiple exocytic proteins to regulate neurotransmitter release in vivo. *Neuron.* 23:593–605.

Wucherpfennig, T., M. Wilsch-Brauninger, and M. Gonzalez-Gaitan. 2003. Role of *Drosophila* Rab5 during endosomal trafficking at the synapse and evoked neurotransmitter release. *J. Cell Biol.* 161:609–624.

Wycisk, K.A., B. Budde, S. Feil, S. Skosyrski, F. Buzzi, J. Neidhardt, E. Glaus, P. Nurnberg, K. Ruether, and W. Berger. 2006a. Structural and functional abnormalities of retinal ribbon synapses due to Cacna2d4 mutation. *Invest. Ophthalmol. Vis. Sci.* 47:3523–3530.

Wycisk, K.A., C. Zeitz, S. Feil, M. Wittmer, U. Forster, J. Neidhardt, B. Wissinger, E. Zrenner, R. Wilke, S. Kohl, and W. Berger. 2006b. Mutation in the auxiliary calcium-channel subunit CACNA2D4 causes autosomal recessive cone dystrophy. *Am. J. Hum. Genet.* 79:973–977.

Yao, J.G., and Y.H. Sun. 2005. Eyg and Ey Pax proteins act by distinct transcriptional mechanisms in *Drosophila* development. *EMBO J.* 24:2602–2612.

Zhai, R.G., P.R. Hiesinger, T.W. Koh, P. Verstreken, K.L. Schulze, Y. Cao, H. Jafar-Nejad, K.K. Norga, H. Pan, V. Bayat, et al. 2003. Mapping *Drosophila* mutations with molecularly defined P element insertions. *Proc. Natl. Acad. Sci. USA.* 100:10860–10865.

Zheng, W., G. Feng, D. Ren, D.F. Eberl, F. Hannan, M. Dubald, and L.M. Hall. 1995. Cloning and characterization of a calcium channel alpha 1 subunit from *Drosophila melanogaster* with similarity to the rat brain type D isoform. *J. Neurosci.* 15:1132–1143.

Zucker, R.S., and W.G. Regehr. 2002. Short-term synaptic plasticity. *Annu. Rev. Physiol.* 64:355–405.